eLife

Reviewed Preprint
v1 • May 18, 2026
Not revised

For correspondence:
yalinzh@nwsuaf.edu.cn
tianzhen@nwsuaf.edu.cn
kingljy0818@hotmail.com

Competing interests: No competing interests declared

Funding: See page 25

Reviewing editor: Hugo J Bellen, Baylor College of Medicine, United States

Metabolic compensation via gluconeogenesis explains the non-essentiality of glycogen phosphorylase as an insecticidal target in *Plutella xylostella*

Yifei Zhou[1], Yanqi Kang[1], Yan Liu[1], Ruichi Li[1], Dongliang Wang[1], Chong Yi[1], Yifan Li[1], Yalin Zhang[1] ✉, Zhen Tian[1] ✉, Jiyuan Liu[1,2] ✉

[1]Key Laboratory of Plant Protection Resources and Pest Management of Ministry of Education, College of Plant Protection, Northwest A&F University, Yangling, China • [2]Northwest A&F University Shenzhen Research Institute, Shenzhen, China

eLife Assessment

This study addresses the mechanism of action of benzoylurea insecticides and explores the metabolic consequences of inhibiting glycogen breakdown in insects. Both reviewers identify major flaws with the premise of the work. The strength of the provided evidence is **inadequate** as the data do not, or poorly, support several central claims. The significance of the findings is considered marginal.

https://doi.org/10.7554/eLife.111144.1.sa3

Abstract

Benzoylphenylurea (BPU) insecticides disrupt insect chitin formation, yet their molecular target is debated. Although resistance-associated mutations map to the Chitin Synthase (*CHS*) gene, direct inhibition of CHS has not been demonstrated. Given the structural similarity of BPUs to mammalian glycogen phosphorylase (GP) inhibitors, GP has been proposed as a potential target controlling chitin precursor flux. We characterized *Plutella xylostella* GP (PxGP) and found that the human GP inhibitor GPI potently inhibits both recombinant PxGP (IC_{50} = 2.96 nM) and native larval GP activity (57.5% reduction), while the BPU diflubenzuron showed no effect. Despite this biochemical inhibition, neither GPI treatment nor RNAi-mediated *PxGP* knockdown (87.6% suppression) caused mortality or developmental defects. Mechanistic analysis revealed coordinated downregulation of glycogenolysis genes (*trehalase* 69%, *hexokinase* 77%) and robust upregulation of gluconeogenolysis genes (*PEPCK* 3.95-fold, *G-6-Pase* 3.34-fold). Critically, protein catabolism (29.4% decline at 72 h) provided substrates for gluconeogenolysis by releasing amino acids. Metabolite profiling validated the full substrate-to-product pathway: transient glucose shortfall was followed by massive accumulation of trehalose (7.4-fold) and glucose-6-phosphate (6.5-fold), confirming a quantitatively sufficient metabolic rescue via *de novo* glucose synthesis. These findings demonstrate that BPUs do not target GP, and that GP inhibition alone is not lethal due to metabolic compensation. This highlights a fundamental metabolic plasticity that must be considered in future target-based insecticide design.

Introduction

The molecular target of benzoylphenylurea (BPU) insecticides—a multi-billion-dollar class of insect growth regulators widely used in agriculture—remains one of the most significant unresolved controversies in insecticide toxicology [1]. Since their introduction over over four

decades ago, BPUs have been known to catastrophically disrupt chitin formation, causing molting failure and larval death [2]. Despite this clear phenotypic effect, their direct molecular target has not been definitively identified, creating a persistent gap between their *in vivo* activity and their presumed mechanism of action.

The prevailing hypothesis posits that BPUs directly inhibit chitin synthase (CHS), the enzyme catalyzing the final polymerization of UDP-N-acetylglucosamine (UDP-GlcNAc) into chitin. This hypothesis is supported by indirect evidence, including the accumulation of UDP-GlcNAc upon BPUs treatment [3] and the genetic co-localization of BPU resistance mutations with the CHS locus in multiple insect species, most notably *Plutella xylostella* [1, 4, 5]. However, direct biochemical studies, beginning with the seminal work by Deul et al. in 1978 [6], have consistently failed to demonstrate CHS inhibition by BPUs in cell-free assays, even at supralethal concentrations [7-9]. This discrepancy between genetic association and enzymatic dataology argues against it—represents an unresolved paradox that has significant implications for understanding BPUs resistance mechanisms and for rational insecticide design.

A largely overlooked clue may help resolve this contradiction: the core acylurea structure of BPUs (Figure 1) closely resembles that of potent inhibitors of mammalian Glycogen Phosphorylase (GP) developed as therapeutic agents for type 2 diabetes [10, 11]. GP catalyzes the rate-limiting step of glycogenolysis, the phosphorolytic cleavage of glycogen to glucose-1-phosphate, which serves as the metabolic gateway controlling flux into the chitin biosynthetic pathway [12]. In insects, this pathway is particularly critical: GP-derived glucose is converted to trehalose (the primary hemolymph sugar), which is subsequently channeled through a series of enzymatic steps to generate UDP-GlcNAc, the substrate monomer for chitin synthesis [13]. GP also plays key roles in carbohydrate homeostasis, osmotic regulation, stress adaptation [14-17]. This structural similarity between BPUs and GP inhibitors (GPIs), combined with GP's upstream regulatory position in chitin precursor synthesis, raises a compelling alternative hypothesis: BPUs may exert their insecticidal effects not by inhibiting CHS directly, but by targeting GP and thereby depleting chitin biosynthesis of its essential precursors.

Here, we systematically test this hypothesis and evaluate GP's potential as an insect control target. We cloned, expressed, and biochemically characterized GP from the globally significant agricultural pest *P. xylostella* (PxGP), measured its inhibition by the BPU—diflubenzuron (DFB) and a specific mammalian GPI, and assessed the physiological consequences of GP loss-of-function *in vivo*. Our findings definitively exclude GP as the target of DFB. More significantly, we identify a robust metabolic compensatory response—the upregulation of gluconeogenesis—that completely rescues insects from GP inhibition. This discovery not only explains why GP alone is not a viable insecticidal target but also reveals a principle of metabolic plasticity that must be considered in the design of metabolism-targeting pesticides.

Results

Recombinant *P. xylostella* glycogen phosphorylase (PxGP) is a functional, activatable enzyme

To investigate its biochemical properties and evaluate its potential as an insecticidal target, the full-length *PxGP* cDNA (predicted molecular mass of 98.1 kDa) was cloned and expressed in Sf9 cells using the Bac-to-Bac baculovirus expression system. Following purification via immobilized metal-affinity chromatography (IMAC) of the N-terminal 6×His tagged protein [18], SDS-PAGE analysis and Western blot analysis confirmed a highly pure protein band migrating at approximately 100 kDa, consistent with its theoretical mass (Figure 2A). A total yield of 7.5 mg of purified protein was obtained from 8.25 g of cell pellet (specific yield=0.91 mg/g cells).

Glycogen phosphorylase activity is regulated by reversible phosphorylation, existing as a less-active dephosphorylated b form (PxGP-b) and a fully active phosphorylated a form (PxGP-a) [19]. Recombinant PxGP-b was activated by incubation with immobilized phosphorylase kinase (PhK) in the presence of ATP and Mg^{2+} for 2 h [20]. The activated enzyme showed robust catalytic activity in a coupled-enzyme spectrophotometric assay, with NADPH production (monitored by increase in

Figure 1. Structural comparison of benzoylphenylurea (BPU) insecticides and a mammalian glycogen phosphorylase inhibitor (GPI) reveals a shared acylurea scaffold.

Chemical structures of four BPU insecticides (Diflubenzuron, Teflubenzuron, Novaluron, and Flufenoxuron) and a human glycogen phosphorylase inhibitor (GPI) are shown. All share a central N,N′-diphenylurea (acylurea) core (dashed boxes). BPUs are characterized by halogenated (F, Cl) aromatic substituents and in some cases by additional ether or alkyl side chains. The GPI contains a methoxyphenyl group bearing an additional methylurea side chain. This structural similarity underpinned the hypothesis that insect GP might be a molecular target for BPUs.

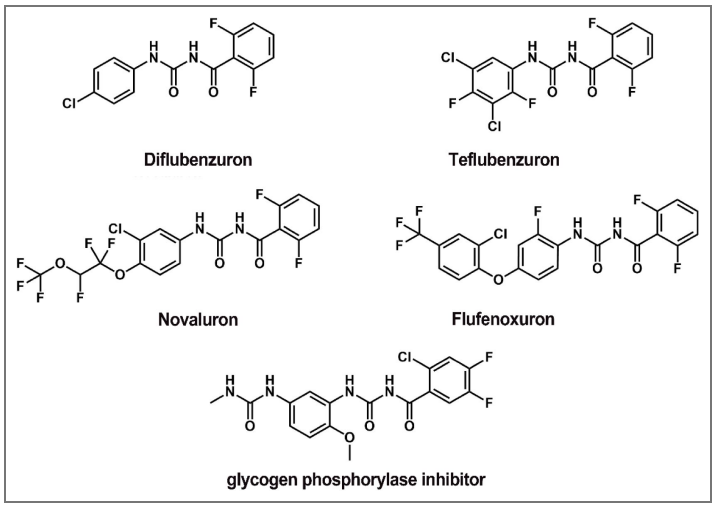

Figure 2. Recombinant PxGP is inhibited by a mammalian GP inhibitor (GPI) but not by the benzoylphenylure Diflubenzuron.

(A) Purification of 6×His-tagged PxGP from Sf9 cells. Left panel: Coomassie-stained SDS-PAGE.. Right: Western blot with anti-His antibody. The expected ~100 kDa band is indicated (red box). M, marker; S, soluble fraction; P, pellet; F, flow-through; lanes 1–4, imidazole elution fractions. (B) Dose-response inhibition by GPI. Activated PxGP-a activity was measured after pre-incubation with GPI (0.16–500 nM). Data (mean ± SEM, n=3) were fit to a four-parameter logistic curve. The calculated IC_{50} is 2.96 nM. *Inset:* GPI structure with its characteristic asymmetric side chains (orange). (C) Inhibition assay with DFB (0.54–1700 nM). DFB did not yield a complete sigmoidal inhibition curve, causing ≤62% inhibition at the highest concentration. *Inset:* DFB structure with its characteristic halogenated benzoyl groups (orange). This rules out PxGP as a direct target of DFB.

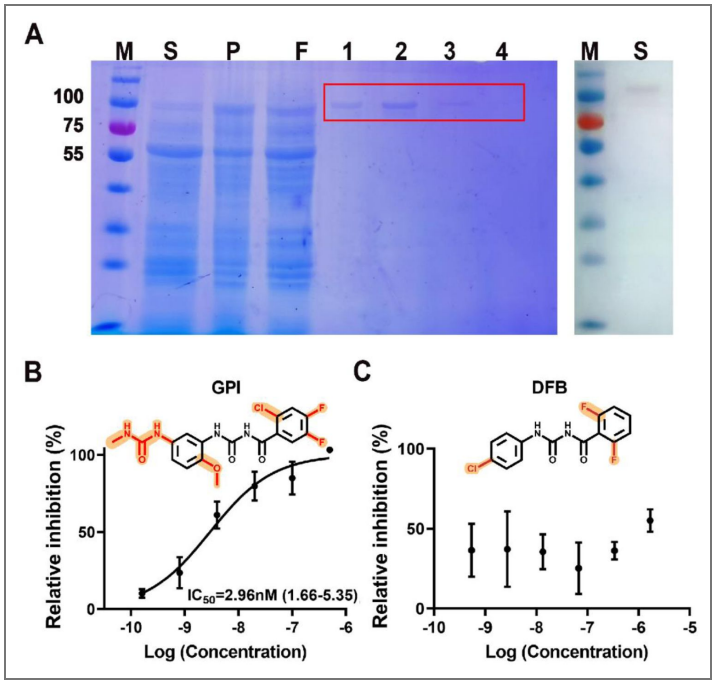

A_{340}) increasing linearly for the first 15 min and reaching a plateau by approximately 20 min, consistent with substrate depletion and/or product accumulation. The specific activity of activated PxGP-a was 294.25 ± 3.45 U/mg protein (Figure S1A), confirming that the recombinant enzyme is catalytically competent for inhibitor screening.

GPI potently inhibits PxGP *in vitro* and *in vivo*

Given the structural similarity between insecticidal BPUs and mammalian GPIs [11] (Figure 1), we tested whether PxGP could be a target of acylurea-scaffold compounds. GPI exhibited potent, dose-dependent inhibition of recombinant PxGP-a, with a sigmoidal dose-response curve typical of competitive or allosteric inhibition (Figure 2B). Non-linear regression analysis yielded an IC_{50} value of 2.96 nM (95% confidence interval [CI]: 1.66–5.35 nM, Hill slope = 0.74, R^2 = 0.877, n = 3). Near-complete inhibition (>95%) was achieved at 500 nM GPI, indicating saturable, high-affinity binding. The potency of GPI against PxGP is comparable to its effect on mammalian orthologs (see below) [11].

In striking contrast, the BPU insecticide Diflubenzuron (DFB), which shares the acylurea core with GPI (Figure 1), did not effectively inhibit PxGP-a. No standard sigmoidal dose-response curve was observed over 0.54 nM to 1700 nM (Figure 2C). Maximum inhibition observed did not exceed 61.96 ± 2.54% (mean ± SEM) even at 100 μM, with high variability at lower concentrations. These data indicate that DFB, unlike GPI, is not an effective inhibitor of PxGP, ruling out GP as the direct molecular target of this BPU insecticide.

Consistent with the recombinant enzyme results, GPI effectively inhibited native GP activity in crude lysates from third-instar larvae in a dose- and time-dependent manner (Figure S1B). After 45 min of pre-incubation, 10 μM GPI reduced native GP activity by 57.52 ± 1.88% (n = 3). DFB, however, showed no significant inhibitory effect on native GP activity at any concentration tested (10^{-7}, 10^{-6}, or 10^{-5} M) or time point (5, 10, 20, or 30 min), with activity remaining at 97-108% of control (Figure S1C).

Collectively, these results establish PxGP as a high-affinity molecular target for GPI but definitively exclude it as a target for DFB. This resolves the primary hypothesis by demonstrating that BPUs do not inhibit insect glycogen phosphorylase.

Paradoxical finding: potent PxGP inhibition by GPI lacks *in vivo* toxicity

Because GPI potently inhibit PxGP, the rate-limiting enzyme in glycogenolysis, which supplies precursors for chitin synthesis [21], we expected it to exhibit significant insecticidal activity. In leaf-dip bioassays with third-instar *P. xylostella* larvae continuously exposed to GPI (250 or 500 mg/L) or DFB (125 or 250 mg/L), GPI caused no significant toxicity or developmental disruption across the entire time course (24 to 120 h post-treatment) (Figure 3A). At 120 h, mortality with 500 mg/L GPI was only 12.78 ± 2.42% (n = 3), which was not significantly different from the solvent control (CK: 5.00 ± 5.00%, P = 0.21) (Figure 3B). Larvae exposed to 250 mg/L GPI exhibited even lower mortality (2.50 ± 2.50%).

In stark contrast, DFB induced significant, dose-dependent mortality. At 120 h, DFB treatment at 125 mg/L caused 41.60 ± 4.85% mortality (P < 0.01 vs. control) and at 250 mg/L caused 61.36 ± 10.02% mortality (P < 0.01 vs. control). Probit analysis of the DFB dose-response data yielded calculated LC_{30} and LC_{50} values of 141.900 mg/L (95% CI: 67.893–206.576 mg/L) and 229.537 mg/L (95% CI: 145.287-331.784 mg/L), respectively, with an acceptable goodness-of-fit (χ^2 = 11.946, P = 0.683) (Table S2).

Furthermore, GPI-treated larvae showed no developmental abnormalities. Pupation rates were 64.17 ± 4.79% for the 500 mg/L GPI group and 69.72 ± 6.81% for the 250 mg/L group, which were statistically indistinguishable from the control group (64.72 ± 9.33%, P > 0.05 for both comparisons) (Figure 3B, middle panel). Similarly, adult emergence rates were 56.11 ± 5.64% and 56.39 ± 6.24% for the 500 and 250 mg/L GPI groups, respectively, compared to 54.10 ± 11.91 % for the control (P > 0.05, Figure 3B). Phenotypically, GPI-treated larvae molted normally, fed

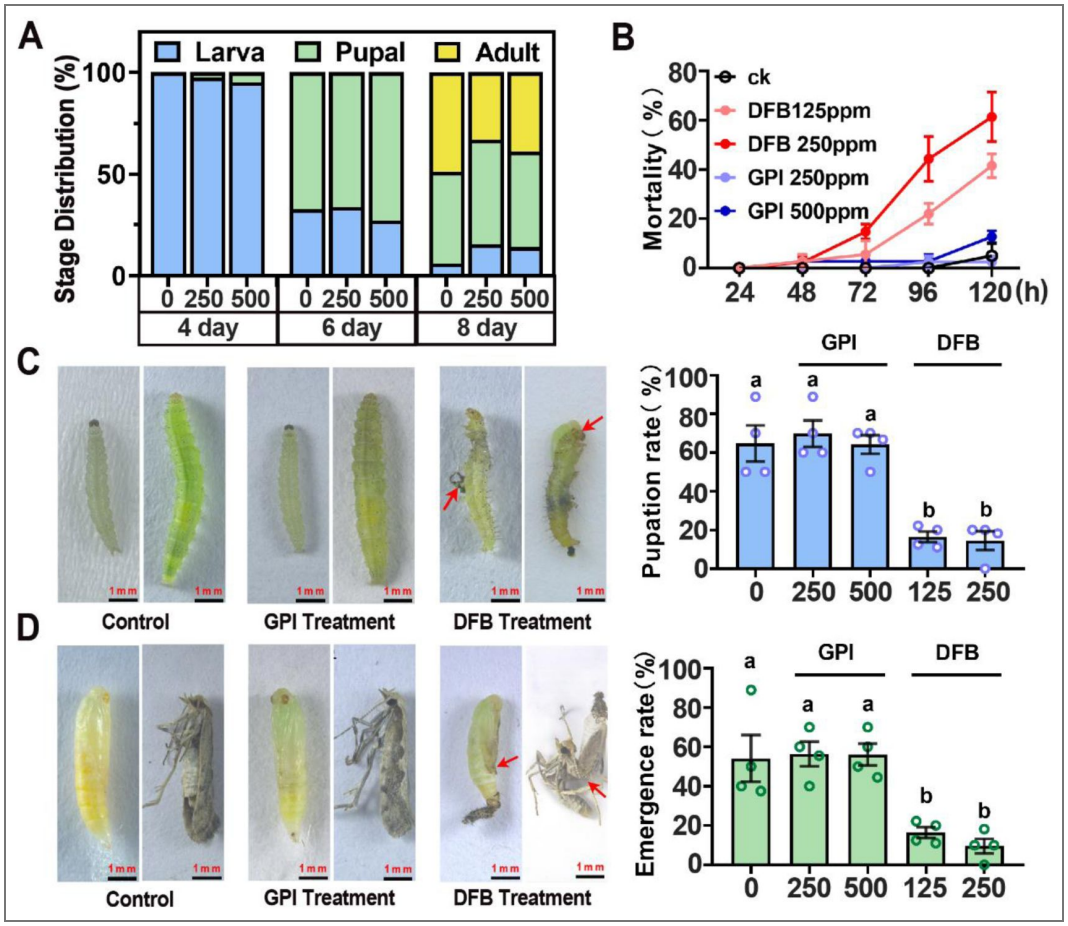

Figure 3. The GP inhibitor (GPI) is non-toxic to *Plutella xylostella*, unlike the benzoylphenylurea Diflubenzuron (DFB).

(A) Developmental stage distribution over time for control, GPI (250, 500 mg/L), and DFB (125, 250 mg/L) treated larvae. DFB causes developmental arrest. (B) Quantitative effects on mortality (top), pupation (middle), and adult emergence (bottom). GPI groups did not differ from control ($P > 0.05$), whereas DFB caused significant, dose-dependent mortality and severely impaired development (*$P < 0.05$). Data are mean ± SEM (n=3). Different letters denote statistical significance. (C) Larval phenotypes at 96 h. Control and GPI-treated larvae are normal. DFB-treated larvae show catastrophic molting failure and "double cuticle" (red arrows). Scale bar, 1 mm. (D) Pupal and adult phenotypes. GPI- treated individuals develop normally. DFB treatment results in deformed pupae and trapped pharate adults (red arrows). Scale bar, 1 mm.

actively, and displayed no cuticle defects (Figure 3C). DFB-treated larvae exhibited the characteristic phenotypes of BPU intoxication: catastrophic molting failure, larval-pupal intermediates, and complete failure of adult emergence (Figure 3C and 3D). This striking discrepancy between biochemical potency and *in vivo* inefficiency presents a profound paradox that demands mechanistic investigation.

GPI exposure triggers a compensatory upregulation of *PxGP* transcription

To explore this discrepancy, we measured *PxGP* gene expression after GPI exposure. RT-qPCR revealed that 500 mg/L GPI rapidly upregulated *PxGP* mRNA transcription. As shown in Figure 4, its relative expression increased 3.24-fold at 24 h, peaked at 3.48-fold at 48 h, and remained elevated at 96 h. This indicates that the insect responds to the pharmacological inhibition by transcriptionally increasing the *de novo* synthesis of the target enzyme.

Sequence homology and rationale for target site selection

To achieve effective gene knockdown coupled with functional ablation, precise selection of the interference target site is critical. Sequence analysis of PxGP (837 residues) revealed that residues 88-680 form the active site pocket of the GT35_Glycogen_Phosphorylase family, and the C-terminal region contains a phosphatase-pyridoxal phosphate linkage site (residues 672-684). Eleven residues within positions 42-318 are conserved and correspond to the AMP-binding site in human GP (Figure 5A) [22].

Multiple sequence alignment of PxGP with GP orthologs from other key lepidopteran pests (*Helicoverpa armigera* HaGP, *Spodoptera exigua* SeGP, *Ostrinia furnacalis* OfGP), human (HsGP), and rabbit (OcGP) demonstrated high conservation across species (Figure 5B). PxGP shares 82.29% sequence identity with human GP (Figure S2). Since GP activity is allosterically regulated by AMP binding and phosphorylation at Ser14, triggering a conformational shift from the inactive T-state GPb (unphosphorylated) to the active R-state GPa (phosphorylated) [19], we targeted the core AMP-binding site region (gray box in Figure 5B) for RNAi. Theoretically, interference in this region should prevent AMP-mediated activation of existing GPb while degrading the entire mRNA pool, drastically reducing total GP protein synthesis and ensuring complete functional ablation.

RNAi confirms PxGP is non-essential for larval development

The compensatory upregulation of PxGP mRNA expression in response to pharmacological inhibition (Section 3.4) indicated that the gene is under active transcriptional regulation and suggested that increased enzyme synthesis might partially mitigate the effects of GPI. However, this compensation alone could not fully explain the complete absence of phenotype. To determine whether a more profound loss-of-function—achieved by directly suppressing *PxGP* gene expression—is lethal, we performed RNAi to knock down *PxGP* at the transcriptional level.

Firstly, we quantified the expression profile of *PxGP* across developmental stages in *P. xylostella*, *PxGP* was highly expressed in fourth-instar larvae (L4) and adults (Figure 6), stages that correlate with the energy demands for metamorphosis and flight, respectively [12, 23]. Given the inherent time lag required for systemic dsRNA delivery to achieve effective post-transcriptional knockdown [24], dsRNA was administered during the mid-third-instar larval stage. Mid-third-instar larvae were microinjected with dsRNA targeting a conserved 606 bp region of *PxGP* (ds*GP*) or with a non-specific control ds*GFP*. Three concentrations of ds*GP* (6,000, 10,000, and 14,000 ng/μL) were tested, and knockdown efficiency was assessed by RT-qPCR at 24, 48, 72, and 96 h post-injection (Figure 7). The highest concentration (14,000 ng/μL) achieved maximal suppression at 48 h, reducing *PxGP* transcript levels to 12.47 ± 1.68% of the ds*GFP* control (87.59% knockdown, $P < 0.001$) (Figure 7B). Significant knockdown persisted at 72 h (69.86% suppression,$P < 0.05$), with partial recover by 96 h, likely due to dsRNA degradation and/or compensatory transcriptional upregulation. The 10,000 ng/μL dose also produced significant knockdown at 48 h (65.76% suppression, $P < 0.01$), whereas the 6,000 ng/μL dose showed more modest effects (Figure 7B).

Figure 4. Ingestion of GP inhibitor (GPI) induces compensatory upregulation of *PxGP* transcription.

Relative *PxGP* mRNA levels in larvae after continuous exposure to 500 mg/L GPI or control (CK). Expression was normalized to *PxRPS13* (control set to 1.0 at each time point) using the $2^{-\Delta\Delta Ct}$ method. Data are mean ± SEM (n=3). GPI triggered a rapid and sustained transcriptional increase, peaking at 48 h (3.48-fold). Significance vs. control: **P* < 0.05, ***P* < 0.01, ****P* < 0.001 (two-way ANOVA with Sidak's test).

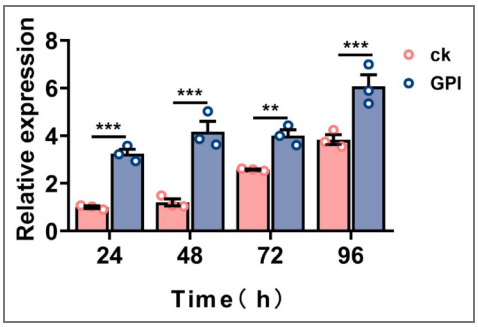

Figure 5. PxGP sequence conservation and domain architecture.

(A) Schematic of PxGP functional domains: pyridoxal phosphate (PLP) binding site (blue boxes), AMP allosteric site (yellow boxes), and glycogen-binding/active site pocket (blue shading). (B) Multiple sequence alignment of GP from *Plutella xylostella* (PxGP), other lepidopterans (*Helicoverpa armigera* HaGP, *Spodoptera exigua* SeGP, *Ostrinia furnacalis* OfGP), human (HsGP), and rabbit (OcGP). Identical residues are shaded red. The gray box indicates the 606 bp region (aa 22–224) targeted for RNAi, which overlaps the conserved AMP-binding domain. PxGP shares 82.29% identity with human GP.

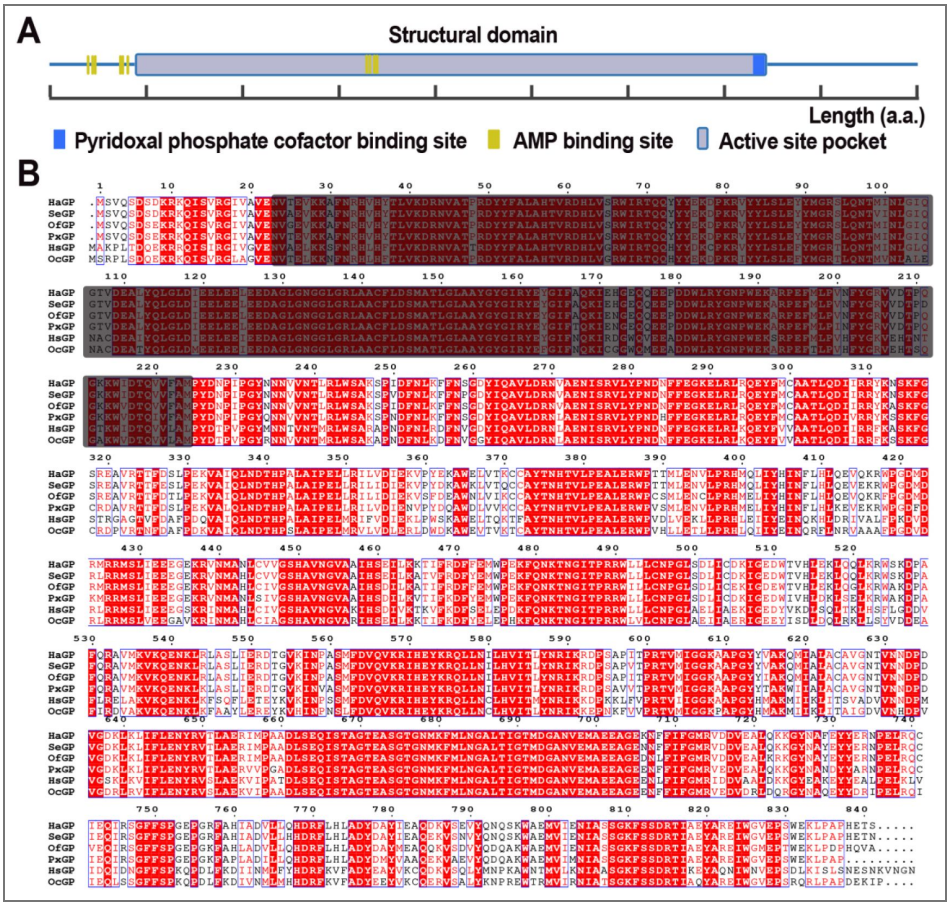

Figure 6. Developmental expression profile of *PxGP*.

Relative *PxGP* mRNA levels across life stages (Egg, larval instars L1-L4, Pupa, Adult), normalized to *PxRPS13* (L1 set to 1.0). Data are mean ± SEM (n=3). Expression peaks in adults. Different letters indicate significant differences ($P < 0.05$, one-way ANOVA with Tukey's test).

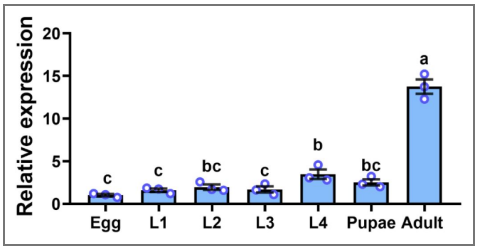

Figure 7. RNAi-mediated knockdown of *PxGP* is dose- and time-dependent.

(A) Experimental workflow. Third-instar larvae were injected with dsRNA targeting *PxGP* (ds*GP*) at three concentrations or a control dsRNA (ds*GFP*), then sampled for analysis. (B) Time-course of *PxGP* mRNA levels post-injection, relative to ds*GFP* control (set to 1.0). The highest ds*GP* dose (14,000 ng/μL) caused maximal suppression (87.6%) at 48 h. Data are mean ± SEM (n=3). Significance vs. ds*GFP* at each time point: $^{**}P < 0.01$, $^{***}P < 0.001$ (one-way ANOVA with Tukey's test).

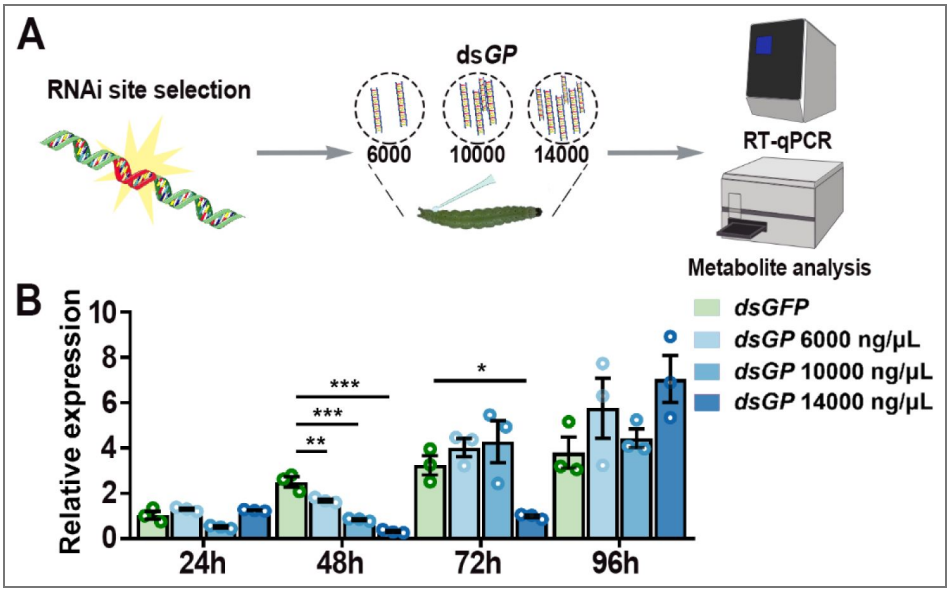

Despite this robust, transient silencing, no adverse phenotypic effects were observed. Developmental stage distribution and mortality rates in all ds*GP*-treated groups (6,000, 10,000, and 14,000 ng/μL) were statistically indistinguishable from the ds*GFP* control group across the entire 120 h observation period ($P > 0.05$ at all time point) (Figure 8A and 8B). At 120 h, cumulative mortality was 8.10 ± 4.23%, 9.82 ± 0.81%, and 3.33 ± 3.33% for the 6,000, 10,000, and 14,000 ng/μL ds*GP* groups, respectively, comparable to the ds*GFP* control (Figure 8B). Pupation and adult emergence also indistinguishable from controls (Figure 8B). Phenotypic examination revealed that ds*GP*-injected larvae developed normally, molted successfully, formed morphologically normal pupae, and emerged as viable adults without cuticle defects or developmental delays (Figure 8C and 8D). Thus, acute, profound suppression of *PxGP* expression is not lethal to *P. xylostella* during the critical larval-pupal transition, despite the enzyme's established role in glycogenolysis and chitin precursor synthesis. This finding necessitates an investigation into the compensatory mechanisms that allow the insect to survive in the absence of functional GP.

PxGP knockdown coordinately suppresses the glycogenolysis-to-chitin pathway

To elucidate how larvae survive GP loss, we examined downstream genes linking glycogenolysis to chitin synthesis. Specifically, we measured the expression of trehalase (*PxTre*), which hydrolyzes circulating trehalose to glucose [12], and hexokinase (*PxHex*), which phosphorylates glucose to glucose-6-phosphate—a key branch point leading to UDP-GlcNAc synthesis for chitin production [25, 26].

RT-qPCR analysis revealed that suppression of *PxGP* triggered a coordinated transcriptional downregulation of both downstream genes (Figure 9A and 9B). At 48 h post-injection, coinciding with the peak of *PxGP* knockdown (87.59% suppression), *PxTre* expression was reduced to 30.46 ± 1.25% of the ds*GFP* control (69.54% suppression, $P < 0.001$,), and *PxHex* to 22.82 ± 3.39% of control (77.18% suppression, $P < 0.001$). This suppression persisted at 72 h (*PxTre*: 61.27 ± 2.21% suppression, $P < 0.001$; *PxHex*: 41.96 ±4.02% suppression, $P < 0.001$) and returned to near baseline levels by 96 h, mirroring the recovery kinetics of *PxGP* itself.

This coordinated downregulation indicates that the insect responds to the loss of GP not by futilely attempting to maintain flux through a pathway that lacks its key upstream enzyme, but rather by implementing a broader transcriptional shutdown of the glycogenolysis-to-glucose-to-chitin pathway. This suggests a coherent metabolic response program, raising the question: if glycogenolysis is blocked, how does the insect obtain the glucose required for survival and chitin synthesis?

Biphasic metabolic response: transient depletion followed by gluconeogenic rescue

The absence of a lethal or developmental phenotype despite glycogenolysis pathway suppression suggested activation of alternative glucose synthesis pathway to compensate for GP loss. We therefore measured expression of key gluconeogenic enzymes and metabolite levels across the glycogeno-glucose axis.

Gene expression analysis reveals gluconeogenic activation

We assessed transcript levels of two rate-limiting gluconeogenic enzymes: phosphoenolpyruvate carboxykinase (PEPCK, encoded by *PxPEPCK*), which catalyzes the conversion of oxaloacetate to phosphoenolpyruvate; glucose-6-phosphatase (G-6-Pase, encoded by *PxG-6-Pase*), which catalyzes the dephosphorylation of glucose-6-phosphate to free glucose. These enzymes are reciprocally regulated relative to glycolysis/glycogenolysis and serve as molecular markers of gluconeogenic flux [27, 28].

At 96 h post-injection—a critical pre-pupal stage with high carbohydrate demand for pupal cuticle synthesis [29, 30]—both *PxPEPCK* and *PxG-6-Pase* were significantly upregulated in ds*GP*-treated larvae (3.95 ± 0.44-fold and 3.34 ± 0.20-fold versus ds*GFP* control, respectively; $P < 0.001$ for each)

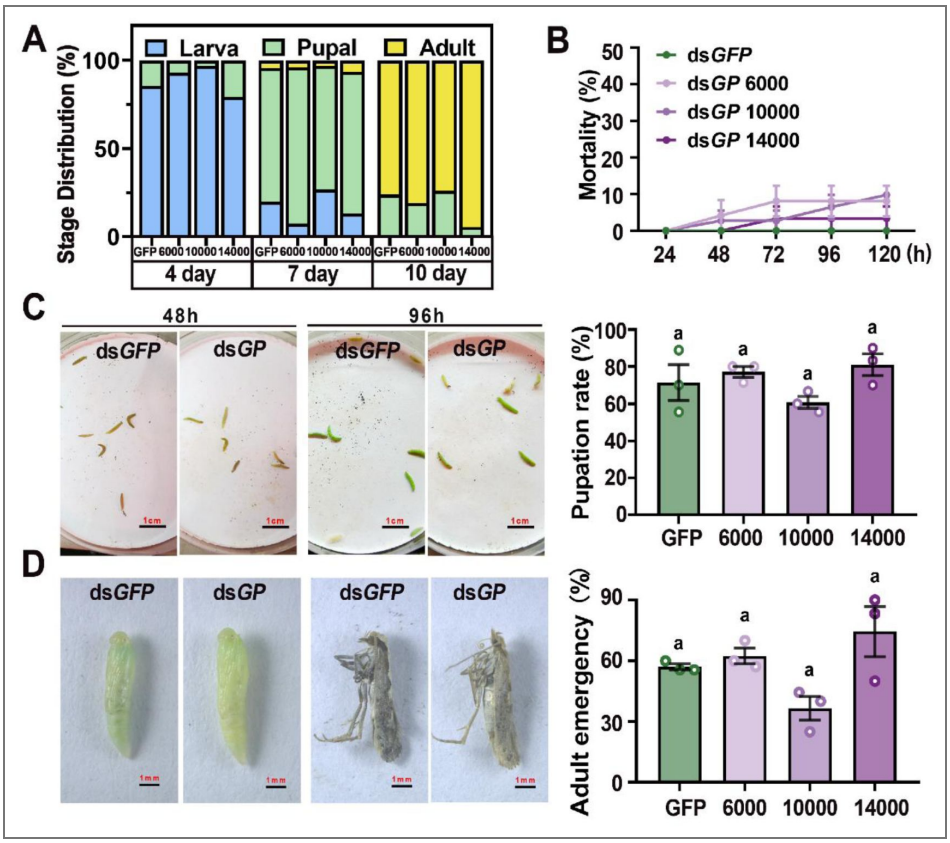

Figure 8. ***PxGP*** **knockdown does not impair development or survival.**

(A) Developmental stage distribution post-injection shows similar progression across all groups. (B) Cumulative mortality (top), pupation (middle), and adult emergence (bottom) rates were not significantly different between ds*GP* and ds*GFP* control groups ($P > 0.05$). Data are mean ± SEM (n=3). (C) Representative larval phenotypes at 48 h and 96 h post-injection are normal in both ds*GFP* and high-dose ds*GP* groups. Scale bar, 1 mm. (D) Pupae and adults from both groups are morphologically normal. Scale bar, 1 mm.

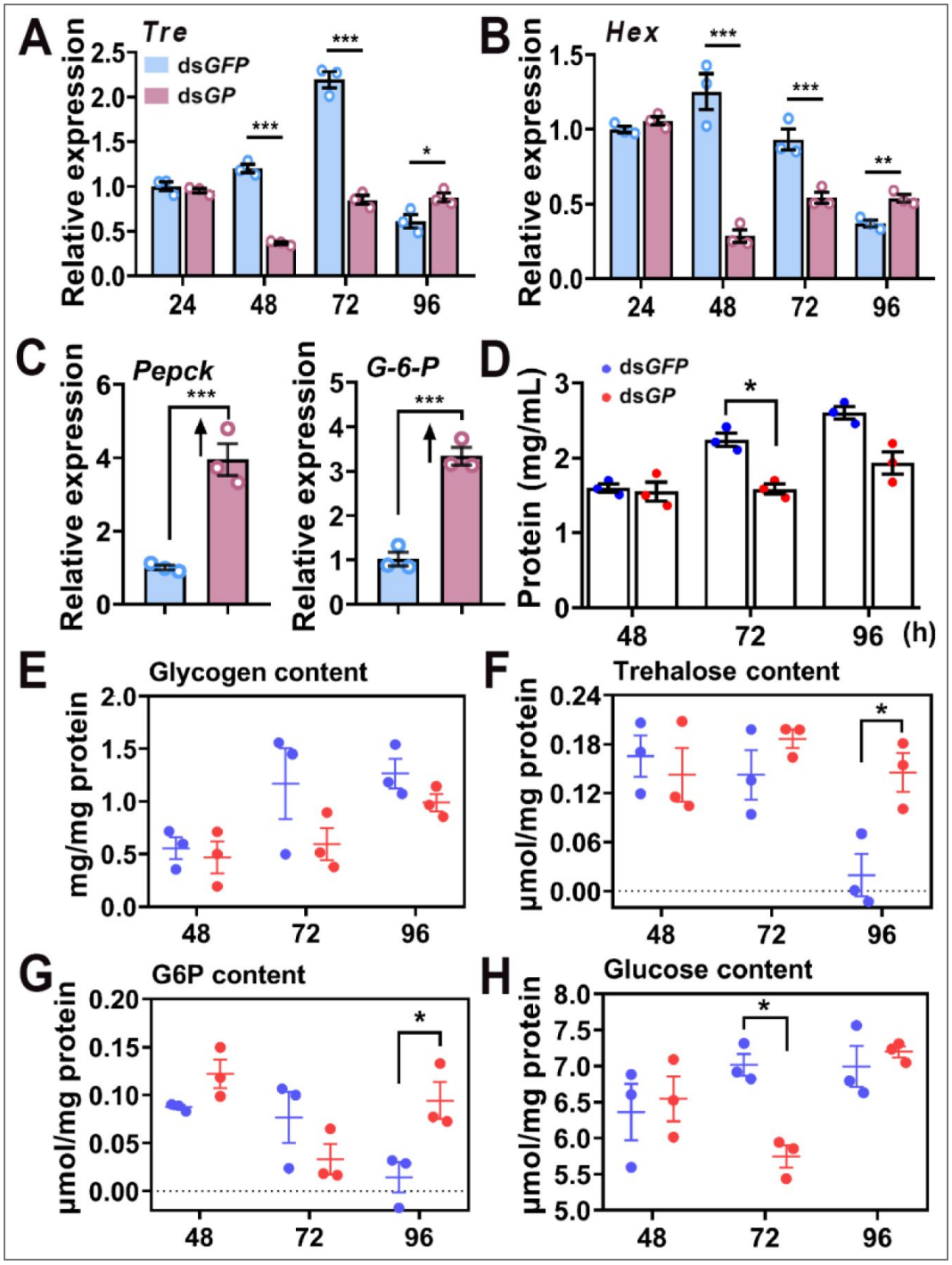

Figure 9. *PxGP* knockdown triggers biphasic metabolic reprogramming, culminating in gluconeogenic compensation.

(A, B) Concurrent suppression of downstream genes *Trehalase (PxTre)* and *Hexokinase (PxHex)* post-knockdown. (C) Upregulation of gluconeogenic genes *PEPCK* and *G6Pase* at 96 h. Data in A-C are mean ± SEM (n=3); **P* < 0.05, ***P* < 0.01, ****P* < 0.001 vs. ds*GFP* control. (D-H) Metabolite levels post-knockdown. (D) Total protein decreased at 72 h (*P* < 0.01). (E) Glycogen remained stable. (F) Trehalose surged 7.4-fold at 96 h (*P* < 0.001). (G) Glucose-6-phosphate (G6P) increased 6.5-fold at 96 h (*P* < 0.001). (H) Free glucose showed a transient dip at 72 h (*P* < 0.05) before recovery. Data are mean ± SEM (n=3); **P* < 0.05, ****P* < 0.001 vs. control at each time point.

(Figure 9C and 9D). This indicates robust transcriptional activation of the gluconeogenesis pathway in response to GP loss.

Protein catabolism provides gluconeogenic substrate mobilization

To identify the carbon source for gluconeogenesis, we quantified total protein content in ds*GP*-treated larvae across the time course. Strikingly, a significant 29.39% reduction in protein was observed at 72 h post-injection ($P < 0.01$), coinciding precisely with the nadir of glucose insufficiency (Figure 9D).

This protein decline provides direct biochemical evidence for substrate mobilization: the degradation of cellular proteins liberates amino acids, which serve as the primary carbon source for gluconeogenesis in insects [27, 31-33]. The magnitude of protein loss (~30%) is sufficient to provide substantial amino acid flux into the gluconeogenic pathway.

Metabolite profiling reveals a biphasic adaptation

Quantification of four key metabolites (glycogen, trehalose, glucose-6-phosphat [G6P], and free glucose) along the glycogen-glucose axis at 48, 72, and 96 h post-injection uncovered a dynamic, biphasic response (Figure 9E-9H).

1. Glycogen Content: Contrary to the expectation of accumulation upon GP blockade, glycogen levels remained unchanged relative to controls throughout the time course ($P > 0.05$) (Figure 9E). This paradox indicates that insects activate alternative, GP-independent pathways for glycogen catabolism—most likely via α-amylase or glycogen debranching enzymes [34-36]—to provide emergency glucose mobilization during the period of metabolic stress, suggesting that these compensatory pathways are sufficient for short-term energy needs but are eventually superseded by gluconeogenic glucose production.
2. Trehalose: Trehalose levels remained stable at 48-72 h but surged dramatically by 96 h (7.44-fold elevation, $P < 0.001$) (Figure 9F and 9G). This massive accumulation, coinciding precisely with the peak gluconeogenic gene (e.g., *PEPCK* and *G-6-Pase*) expression, indicates that newly synthesized glucose derived from gluconeogenesis is being actively channeled into trehalose synthesis. The magnitude of this accumulation indicates that gluconeogenic glucose production exceeds the immediate metabolic demands of the larva, creating a metabolic "overshoot" that ensures adequate carbohydrate reserves for the upcoming pupation [37].
3. G6P: G6P, which sits at the intersection of glycolysis, gluconeogenesis, the pentose phosphate pathway, and glycogen synthesis [38], exhibited a pattern mirroring that of trehalose (Figure 9G). G6P content declined gradually from 48 to 72 h, consistent with reduced glucose mobilization from glycogen, but then increased sharply at 96 h (6.49-fold elevation, $P < 0.001$). This surge directly reflects the massive influx of glucose generated via the gluconeogenic pathway, which enters the metabolic network at the G6P node. The coordination between G6P accumulation and trehalose accumulation confirms that gluconeogenesis-derived glucose is being efficiently converted into storage and transport carbohydrates.
4. Free Glucose: Free glucose levels showed the most subtle but perhaps most physiologically informative pattern (Figure 9H). At 48 h—coinciding with peak PxGP suppression—glucose content was statistically indistinguishable from controls ($P > 0.05$), indicating that initial homeostatic mechanisms (including GP-independent glycogen breakdown and dietary carbohydrate absorption) successfully buffer against acute GP loss. However, at 72 h, the nadir of the metabolic stress response, free glucose levels declined significantly, albeit modestly (18.15% reduction, $P < 0.05$). This transient dip reveals a critical window of metabolic insufficiency during which the insect's compensatory mechanisms are insufficient to fully maintain glucose homeostasis. Importantly, by 96 h, glucose levels fully recovered to control values ($P > 0.05$), demonstrating that the gluconeogenic pathway successfully restores glucose homeostasis before critical developmental transitions occur.

Integrated interpretation

Collectively, these metabolite and gene expression data reveal a sophisticated, biphasic metabolic adaptation strategy that fully explains the paradox of why profound GP loss (87.59% knockdown) causes no mortality or developmental defects:

1. Phase I (emergency compensation, 48-72 h): Metabolic stress and emergency compensation during the initial response to PxGP suppression, the insect experiences genuine metabolic stress, evidenced by the glycogen levels neither accumulated nor were depleted and the transient reduction in free glucose at 72 h. The static glycogen content indicates activation of GP-independent catabolism pathways, which provide emergency glucose but are insufficient for complete homeostatic maintenance.The modest glucose dip at 72 h demonstrates that this stress is real but tolerable, likely due to several factors: (i) the magnitude is modest (only 18.15% reduction), (ii) the duration is brief (~24 h), (iii) the timing coincides with the mid-L4 larval stage when energy demands are moderate and active feeding allows dietary carbohydrate supplementation, and (iv) trehalose stores (which remain stable during this phase) can be mobilized to buffer hemolymph glucose.
2. Phase II (gluconeogenic rescue, 96 h): Robust transcriptional upregulation of *PEPCK* and *G-6-Pase* (3-4-fold increases) drives massive de novo glucose synthesis from non-carbohydrate precursors such as amino acids, lactate, and glycerol. The surge of gluconeogenesis-derived glucose is rapidly converted into trehalose and G6P, creating a metabolic overshoot that restores basal glucose levels. This overcompensation ensures adequate carbohydrate supply for the energetically demanding process of pupal cuticle synthesis, which begins shortly after 96 h.

This substrate-to-product chain for gluconeogenesis-mediated metabolic rescue—protein degradation → amino acid release → gluconeogenic conversion → glucose synthesis → trehalose storage—constitutes a complete compensatory mechanism that sustains development despite profound GP ablation.

Discussion

Resolving a long-standing controversy: BPUs do not target GP

A central challenge in mechanism-based insecticide development is distinguishing potent *in vitro* biochemical inhibitors from physiologically effective *in vivo* toxicants. This study addresses this challenge by investigating the debated molecular target of BPU insecticides. For over 40 years, the field has contented with conflicting evidence: while genetic studies implicated chitin synthase [5], direct biochemical assays consistently failed to validate it as a direct BPU target [6, 39, 40]. The structural similarity between BPUs and mammalian GPIs proposed an alternative hypothesis that BPUs might inhibit insect GP, thereby limiting glucose-derived precursors for chitin synthesis. Our systematic investigation demonstrates that while a human GPI potently inhibits PxGP, the BPU insecticide diflubenzuron does not. This discrepancy is attributable to key substitutions in its aromatic halogen substituents, which preclude effective binding to GP's active or allosteric sites. This provides the first direct biochemical evidence excluding GP as a candidate molecular target for BPUs. Consequently, BPU lethality must arise from a different mechanism, likely involving interference with chitin assembly, cuticle organization, or CHS trafficking rather than direct enzymatic inhibition, a mechanism that remains to be conclusively identified [21, 39, 40].

Metabolic plasticity and gluconeogenic compensation underlie GP non-essentiality

The resolution of the BPU target question raised a more profound and unexpected puzzle: despite being a potent GP inhibitor *in vitro*, the GPI exhibited no insecticidal activity *in vivo*. This paradox —wherein a nanomolar-potency inhibitor of a putatively essential metabolic enzyme causes no phenotype—demanded mechanistic investigation.

Our investigation shows that this tolerance stems from a robust, developmentally-coordinated metabolic compensation mechanism. Even acute RNAi-mediated suppression of *PxGP* expression (87.59% knockdown) induced no discernible phenotype, as insects activated a compensatory gluconeogenic pathway. This was evidenced by the concerted suppression of downstream glycogenolytic enzymes and, crucially, the significant upregulation of the key gluconeogenic enzymes *PEPCK* (3.95-fold) and *G-6-Pase* (3.34-fold) at 96 h post-knockdown. This response provides a metabolic "escape route," synthesizing glucose *de novo* from non-carbohydrate precursors to bypass the blocked glycogenolytic pathway and maintain homeostasis, particularly during the high carbohydrate demand preceding metamorphosis. Future work utilizing transcriptomic and proteomic approaches will be essential to delineate the signaling pathways (potentially involving nutrient sensors like AMPK and transcription factors such as FOXO) that link GP suppression to this precise reprogramming of metabolic gene expression [41, 42].

Direct metabolite quantification validated this compensation and revealed its sophisticated temporal dynamics. The most striking finding was the lack of glycogen accumulation upon *GP* knockdown, a paradox explained by the activation of GP-independent glycogen catabolism via alternative enzymes like α-amylase (which hydrolyzes internal α-1,4-bonds) and glycogen debranching enzymes (which hydrolyze α-1,6-branch points) [34-36]. Definitive metabolic rescue emerged at 96 h, characterized by a dramatic surge in trehalose and G6P, directly driven by the 3-4-fold upregulation of *PEPCK* and *G-6-Pase,* providing definitive biochemical proof that *de novo* glucose synthesis is the primary rescue mechanism. This biphasic response—initial metabolic stress followed by delayed (48-72 h), robust compensation—creates a temporal buffer (96 h), explaining the absence of phenotypes despite severe GP knockdown. This temporal coordination suggests a programmatically timed, possibly hormonally regulated response that anticipates developmental energy needs. Critically, it reveals a metabolic vulnerability window (~72 h); strategies that disrupt both glycogenolysis and gluconeogenesis simultaneously could overcome this compensation.

Implications for insecticide target selection: metabolic redundancy and the dual-target strategy

Our findings offer direct and actionable insights for the rational design of metabolism-targeting insecticides. A key lesson is that the viability of a metabolic enzyme as an insecticidal target is determined not solely by its biochemical function or pathway position but by the presence of compensatory metabolic routes. GP fails as a standalone target due to compensation via gluconeogenesis. This contrasts sharply with other carbohydrate-metabolizing enzymes that have proven to be highly effective insecticidal targets. For example, trehalase inhibitors such as Validamycin A are potent insecticides [43, 44], suggests that inhibition of trehalase does not cause other pathways to initiate glucose compensation. This distinction informs a refined strategy: dual-target inhibition. Simultaneously blocking both glycogenolysis (via GP) and gluconeogenesis (e.g., via PEPCK or G-6-Pase) would create irreversible glucose starvation, a "metabolic pincer" attack that could overcome adaptive compensation—a strategy with precedent in cancer therapy targeting both glycolysis and oxidative phosphorylation [45, 46]. Ultimately, our work highlights the value of systems-level metabolic modeling for target prioritization. Enzymes at metabolic branch points with redundant outputs are less vulnerable than those in non-bypassable pathways (e.g., chitin synthase, trehalase). Prospective application of computational flux balance analysis and constraint-based modeling, as supported by existing literature, can systematically identify such non-compensatable nodes for effective target selection [47].

Study limitations and future directions

We acknowledge several limitations that point to productive future investigations. First, the transient nature of RNAi-mediated gene silencing in Lepidoptera precluded assessment of long-term or stage-specific consequences of GP loss; its role in adult flight or reproduction warrants investigation via CRISPR/Cas9 knockout or advanced dsRNA delivery systems [48-50]. Second, the generalizability of the this gluconeogenic compensation mechanism across insect orders (e.g.,

Coleoptera, Diptera) remains to be tested, as metabolic regulation can vary with ecology and life history. Third, while our multi-layered evidence—from transcriptional upregulation to phenotypic rescue—provides robust qualitative support for the activation of gluconeogenesis, future studies employing ^{13}C-isotope tracer analysis would be valuable to quantify the precise metabolic rates identify primary carbon precursors, and further refine potential metabolic targets for insecticide development [51].

Concluding remarks

In conclusion, our study definitively rules out GP as the target of BPU insecticides, resolving a long-standing controversy. More importantly, it uncovers a fundamental principle of insect metabolic biology: robust compensatory pathways, specifically gluconeogenesis, can buffer against the loss of key catabolic enzymes. This metabolic plasticity renders GP non-viable as a standalone insecticidal target but illuminates a strategic path forward: the development of dual-target inhibitors that simultaneously block glycogenolysis and gluconeogenesis. Our findings underscore the necessity of adopting a systems-level perspective in target-based insecticide discovery. Biochemical potency *in vitro* is necessary but not sufficient for *in vivo* efficacy; the latter requires consideration of metabolic network architecture, pathway redundancy, and compensatory mechanisms. As the pest management community confronts the twin challenges of insecticide resistance and environmental sustainability, this mechanistic understanding of metabolic robustness will be essential for designing the next generation of selective, effective and durable insect control agents.

Materials and Methods

Insects and rearing conditions

A susceptible laboratory strain of *P. xylostella* (L.), maintained for multiple generations at the College of Plant Protection, Northwest A&F University, without prior insecticide exposure, was used for all experiments. Larvae were reared on radish (*Raphanus sativus*) seedlings grown in vermiculite. Adults were provisioned with a 10% (w/v) honey solution. All insect stages were maintained in a controlled environment at 25 ± 1°C, 60 ± 5% relative humidity (RH), and under a 16:8 h (light:dark) photoperiod.

Cell culture and maintenance

Spodoptera frugiperda (Sf9) cells (Gibco, CA, USA) were cultured in Sf-900™ III SFM medium (Gibco) supplemented with 10% fetal bovine serum (FBS; Gibco) and 1% (v/v) Antibiotic-Antimycotic solution (Gibco, Cat# 15240062). Adherent monolayer cultures were maintained in T-flasks at 27°C. For large-scale protein expression, cells were adapted to suspension culture in baffled flasks, agitated at 120 rpm at 27°C. Cells were harvested by centrifugation (4,000 rpm, 10 min, 4°C) when the density reached 5.0×10^6 cells/mL. Cell pellets were flash-frozen in liquid nitrogen and stored at -80°C until use.

Chemicals and reagents

Diflubenzuron (DFB, 1-(4-chlorophenyl)-3-(2,6-difluorobenzoyl) urea, ≥98% purity) was purchased from Shanghai Topscience Co., Ltd. (Shanghai, China, Cat# T0109).

The Glycogen phosphorylase-IN-1 (GPI), 1-(3-(3-(2-Chloro-4,5-difluorobenzoyl)ureido)-4-methoxyphenyl)-3-methylurea (also known as compound 42 in ref [11]), was purchased from TargetMol (Shanghai, China, Cat# T37577, ≥98% purity).

Glycogen (from bovine liver, Type III), β-glycerophosphate, HEPES, imidazole, EDTA, DTT, ATP, $MgCl_2$, protease inhibitor cocktail components (AEBSF, Pepstatin A, Leupeptin), and all other biochemical reagents were purchased from Sigma-Aldrich (Shanghai, China) or Sangon Biotech (Shanghai, China) and were of molecular biology grade (≥95% purity) unless otherwise specified.

Recombinant PxGP expression and purification

The full-length coding sequence of PxGP (2,511 bp, encoding 837 amino acids; GenBank Accession No. XM_038119125.2 was amplified from *P. xylostella* third-instar larval cDNA by PCR using gene-specific primers (Table S1), and cloned into the pFastBac1 vector (Invitrogen, Carlsbad, CA, USA) using homology-based cloning (ClonExpress II One Step Cloning Kit, Vazyme, Nanjing, China). The construct was engineered to express PxGP with an N-terminal 6×His tag (HHHHHH-) immediately following the initiating methionine, under the control of the polyhedrin (PH) promoter. The sequence fidelity of the construct was verified by Sanger sequencing (Tsingke Biotechnology, Beijing, China).

The sequence-verified pFastBac1-PxGP construct was transformed into DH10Bac™ competent cells (Invitrogen) to generate recombinant bacmid DNA via Tn7-mediated transposition, following the manufacturer's Bac-to-Bac® protocol. Recombinant bacmid DNA was isolated, verified by PCR using M13 forward and reverse primers (Table S1), and transfected into Sf9 cells using Cellfectin® II Reagent (Invitrogen) to generate P0 viral stock. The viral titer was amplified through two additional passages (P1, P2) to obtain high-titer P3 viral stock.

For large-scale protein production, Sf9 cells in suspension culture (2.0×10^6 cells/mL, 500 mL culture volume in a 2-L baffled Erlenmeyer flask) were infected with P3 viral stock at a Multiplicity of Infection (MOI) of 5. Infected cultures were maintained at 27°C with agitation at 120 rpm. Cells were harvested 72 h post-infection by centrifugation (4,000 rpm, 10 min, 4°C), yielding approximately 8.25 g of cell pellet. Cell pellets were flash-frozen in liquid nitrogen and stored at -80°C until use.

For protein purification, frozen cell pellets were thawed on ice and resuspended in ice-cold Lysis Buffer (50 mM β-glycerophosphate [pH 7.5], 150 mM NaCl, 0.2 mM DTT, 0.5 mM EDTA, and 1× protease inhibitor cocktail [1 mM AEBSF, 15 μM Pepstatin A, 20 μM Leupeptin]) at a ratio of 4 mL buffer per gram of cell pellet. Cells were lysed by sonication on ice using a Scientz-IID sonicator (Ningbo Scientz Biotechnology, China) with the following parameters: 6 cycles of 30 s ON / 60 s OFF at 40% amplitude. The lysate was clarified by centrifugation (16,000 × g, 30 min, 4°C).

The clarified supernatant was loaded onto a 5-mL HisTrap™ HP column (GE Healthcare, Uppsala, Sweden) pre-equilibrated with Lysis Buffer containing 10 mM imidazole. The column was first washed with 10 column volumes (CV) of Equilibration Buffer (Lysis Buffer + 10 mM imidazole), followed by 5 CV of Wash Buffer (Lysis Buffer + 30 mM imidazole). Bound 6×His-tagged PxGP protein was eluted with a 15 CV linear gradient from 30 to 200 mM imidazole in Lysis Buffer. Fractions (2 mL each) were collected and analyzed by 13% SDS-PAGE with Coomassie Brilliant Blue R-250 staining. Fractions containing PxGP, identified as a prominent band at ~100 kDa, were pooled and dialyzed overnight at 4°C against Storage Buffer (50 mM HEPES [pH 7.4], 150 mM NaCl, 1 mM DTT, 10% [v/v] glycerol) using a 10 kDa molecular weight cut-off dialysis membrane (Spectrum Labs, Rancho Dominguez, CA, USA), with three buffer changes. Protein concentration was determined using the Pierce™ BCA Protein Assay Kit (Thermo Fisher Scientific, Waltham, MA, USA) with bovine serum albumin (BSA) as the standard. Aliquots of purified PxGP were flash-frozen in liquid nitrogen and stored at -80°C. The typical yield was 7.5 mg of purified protein from 8.25 g of cell pellet.

In vitro activation of recombinant PxGP

Purified recombinant PxGP exists predominantly in the inactive dephosphorylated b form (PxGP-b) and requires phosphorylation at a conserved serine residue (corresponding to Ser14 in mammalian GP) for conversion to the active a form (PxGP-a) [19]. Activation was performed *in vitro* using immobilized Phosphorylase Kinase (PhK) (Cat# HY-P2757, MedChemExpress, Monmouth Junction, NJ, USA).

Immobilized PhK beads (100 μL slurry) were washed three times with 1 mL of Kinase Buffer (25 mM β-glycerophosphate, pH 7.5, 0.5 mM EDTA, 0.25 mM DTT, 1× protease inhibitor cocktail) and resuspended in 500 μL of dialyzed PxGP-b solution (final protein concentration: 1 mg/mL). The

activation reaction was initiated by adding ATP (sodium salt) to a final concentration of 7 mM and $MgCl_2$ to 22 mM. The suspension was incubated for 2 h at room temperature (22-25°C) with gentle end-over-end rotation.

Following incubation, the activated PxGP-a (present in the supernatant) was separated from the immobilized PhK beads using a magnetic separation stand. The supernatant was passed through a 0.22 μm syringe filter (Millipore) to remove any residual beads and was used immediately for enzymatic assays. The extent of activation was assessed by measuring specific activity (see Section 2.7). Activated PxGP-a was used fresh and not stored, as phosphorylated GP is subject to dephosphorylation by endogenous phosphatases over time.

Western blot analysis

Protein samples were separated by 13% SDS-PAGE (120 V, 90 min) and electrophoretically transferred to a nitrocellulose (NC) membrane (0.45 μm pore size, Millipore, Burlington, MA, USA) at 300 mA for 90 min at 4°C using a Bio-Rad Mini Trans-Blot® system. The membrane was blocked for 1 h at room temperature in 5% (w/v) non-fat dry milk in TBST (10 mM Tris-HCl, pH 7.4, 150 mM NaCl, 0.1% [v/v] Tween-20).

The membrane was incubated overnight at 4°C with an anti-His mouse monoclonal antibody (1:1500 dilution in blocking buffer; Cat# ABT2050, Abbkine, Wuhan, China). After three washes with TBST (10 min each), the membrane was incubated for 1 h at room temperature with an alkaline phosphatase (AP)-conjugated goat anti-mouse IgG secondary antibody (1:4000 dilution in blocking buffer; Cat# A0208, Beyotime Biotechnology, Shanghai, China). Following three additional TBST washes, immunoreactive bands were visualized using BM Purple AP Substrate (Roche, Basel, Switzerland) according to the manufacturer's instructions. Images were captured using a ChemiDoc™ XRS+ imaging system (Bio-Rad, Hercules, CA, USA).

Glycogen phosphorylase activity assay

GP enzymatic activity was measured using a coupled-enzyme spectrophotometric assay kit (Cat# BC3345, Solarbio Life Science, Beijing, China). This assay quantifies GP activity by measuring the GP-catalyzed phosphorolysis of glycogen to glucose-1-phosphate (G-1-P). The product G-1-P is enzymatically converted to glucose-6-phosphate (G-6-P) by phosphoglucomutase (PGM), and G-6-P is subsequently oxidized by glucose-6-phosphate dehydrogenase (G6PDH), which stoichiometrically reduces $NADP^+$ to NADPH. The rate of NADPH formation, which is directly proportional to GP activity, was monitored by measuring the increase in absorbance at 340 nm (A_{340}) using a Infinite 200 PRO microplate reader (Tecan, Männedorf, Switzerland).

The reaction mixture (200 μL total volume per well in a 96-well UV-transparent microplate) contained the following components (as supplied in the kit): 160 μL of Reaction Buffer (containing glycogen [2 mg/mL final], inorganic phosphate [10 mM], AMP [1 mM], $NADP^+$ [0.4 mM], PGM, G6PDH, $MgCl_2$, and appropriate buffer), 30 μL of deionized water, and 10 μL of enzyme sample (purified PxGP-a or crude larval lysate). The reaction was initiated by adding the enzyme sample, and A_{340} was recorded continuously at 15 s intervals for 30 min at 25°C.

Specific activity was calculated using the following formula:

$$\begin{aligned}&\text{Specific Activity}(\mathrm{U}/\mathrm{mg})\\&=(\Delta \mathrm{A}_{340}/\min)/(\varepsilon\times 1\times[\text{Protein}])\times \mathrm{Vt}/\mathrm{Vs}\times 1000.\end{aligned}$$

where:

ΔA_{340} represents the change in absorbance at 340 nm,

ε = molar extinction coefficient of NADPH at 340 nm (6.22 $mM^{-1} \cdot cm^{-1}$),

l = light path length (0.6 cm for 200 μL in a 96-well microplate),

[Protein] = protein concentration in the assay (mg/mL),

Vt = total reaction volume,

Vs = sample volume added.

One Unit (U) of GP activity is defined as the amount of enzyme that catalyzes the formation of 1 μmol of NADPH per minute under the assay conditions.

Inhibitor screening and IC_{50} determination

For *in vitro* enzyme inhibition assays, purified activated PxGP-a was diluted to 10 μg/mL in Assay Dilution Buffer (30 mM HEPES, pH 7.2, 60 mM KCl, 1.5 mM EDTA, 1.5 mM $MgCl_2$. Test compounds (GPI, DFB) were prepared as 100× stock solutions in DMSO and serially diluted in Assay Dilution Buffer to achieve final assay concentrations ranging from 0.16 nM to 500 nM (for GPI) and 0.54 nM to 1700 nM (for DFB), respectively (final DMSO concentration ≤ 1% [v/v] in all wells, including vehicle controls).

The enzyme (10 μL of 10 μg/mL PxGP-a, final concentration 10 μg/mL in the assay) was pre-incubated with 10 μL of inhibitor solution (or vehicle control) for 15 min at room temperature in a 96-well microplate. The reaction was then initiated by adding 180 μL of the Reaction Buffer (as described in Section 2.7), and A_{340} was monitored continuously for 30 min at 25°C.

Residual enzyme activity at each inhibitor concentration was calculated as a percentage of the vehicle control (1% DMSO alone). Dose-response curves were generated by plotting percent residual activity versus log[inhibitor concentration]. IC_{50} values (the concentration of inhibitor required to reduce enzyme activity by 50%), Hill slopes, and 95% confidence intervals (CI) were calculated by non-linear regression analysis using a four-parameter logistic equation in GraphPad Prism 9.0 (GraphPad Software Inc., San Diego, CA, USA):

$$\mathrm{Y} = \mathrm{Bottom} + (\mathrm{Top} - \mathrm{Bottom}) / \left(1 + 10^{(\mathrm{LogIC}_{50} - \mathrm{X}) \times \mathrm{Hill\ slope}}\right).$$

where Y is percent residual activity, X is log[inhibitor concentration], Top and Bottom are the upper and lower plateaus of the curve (constrained to 100% and 0%, respectively), and Hill slope describes the steepness of the curve.

For each compound, at least three independent experiments were performed, each with triplicate technical replicates.

Preparation of larval crude lysate for *in vivo* activity

To assess the inhibitory effects of GPI and DFB on native GP activity *in vivo*, crude enzyme extracts were prepared from *P. xylostella* larvae. Healthy third-instar (L3) larvae (n = 30 per biological replicate, three replicates total) were collected, briefly washed in ice-cold phosphate-buffered saline (PBS, pH 7.4) to remove surface contaminants, and gently blotted dry on filter paper. Larvae were then homogenized on ice in 3 volumes (w/v) of ice-cold Homogenization Buffer (30 mM HEPES, pH 7.2, 60 mM KCl, 1.5 mM EDTA, 1.5 mM $MgCl_2$, 1× protease inhibitor cocktail).

The homogenate was centrifuged at 15,000 × g for 20 min at 4°C, and the supernatant (crude enzyme extract) was carefully collected, avoiding the lipid layer and pellet. Protein concentration was determined using the BCA assay, and extracts were either used immediately for activity assays or aliquoted and stored at -80°C (activity remained >90% for up to 2 weeks).

GP activity in crude lysates was measured using the same coupled-enzyme assay described in Section 2.7, with the following modifications: crude lysate (diluted to 2 mg/mL total protein) was used in place of purified enzyme, and pre-incubation with inhibitors was performed for 5 to 45 min to assess time-dependent inhibition. Final inhibitor concentrations tested were 10^{-5}, 10^{-6} or 10^{-7} M.

Sequence alignment and bioinformatic analysis

The amino acid sequence of PxGP (XP_037975053.2) was obtained from the NCBI database. Multiple sequence alignment with orthologs from *Homo sapiens* (NP_002854.3), *Oryctolagus cuniculus* (NP_001075653), *Helicoverpa armigera* (XP_021190210.1), *Spodoptera exigua*

(ACN78408.1), and *Ostrinia furnacalis* (AFO54708.2) was performed using ClustalX. Conserved domains and motifs were analyzed using the ScanProsite and NCBI CD-Search web servers. Protein pairwise similarity matrix was visualized as a heatmap using the "HeatMap" module in TBtools-Ⅱ (v2.390) [52].

Larval bioassays

Larval bioassays were conducted using a standard leaf-dip method adapted from established protocols [53]. Stock solutions of GPI and DFB were prepared in HPLC-grade acetone at 10,000 mg/L. Serial dilutions were prepared in deionized water containing 0.1% (v/v) Triton X-100 as a wetting agent to achieve final test concentrations of 250 and 500 mg/L for GPI, and 125 and 250 mg/L for DFB. The final acetone concentration in all treatment solutions was 1% (v/v). A solvent control group (CK) consisted of 1% acetone and 0.1% Triton X-100 in water without any test compound.

Fresh cabbage (*Brassica oleracea* var. *capitata*) leaf discs (5 cm diameter) were cut using a cork borer, dipped in the respective treatment solutions for 6-8 s with gentle agitation, and then air-dried for 30 min at room temperature in a fume hood. Once dry, each leaf disc was placed in a sterile 90 mm petri dish lined with moistened filter paper.

Ten synchronized third-instar larvae of *P. xylostella* (24-36 h post-molt to L3) were transferred to each treated leaf disc using a soft brush. Each treatment consisted of three biological replicates (i.e., three Petri dishes, 30 larvae total per treatment). Petri dishes were sealed with Parafilm® and maintained under standard rearing conditions (25 ± 1°C, 60 ± 5% RH, 16:8 h L:D photoperiod). Leaf discs were replaced with freshly treated discs every 12 h to ensure continuous exposure.

Mortality was recorded every 24 h for 120 h (5 days). Larvae that failed to respond to gentle prodding or showed moribund behavior (inability to right themselves or move coordinately) were considered dead. Corrected mortality was calculated using Abbott's formula [54]:

$$\begin{gathered}\text{Corrected Mortality}(\%) = \\ [(\text{Treatment Mortality} - \text{Control Mortality}) \\ /(100 - \text{Control Mortality})] \times 100\end{gathered}$$

Pupation rates (number of pupae formed / initial number of larvae × 100) and adult emergence rates (number of emerged adults / number of pupae formed × 100) were recorded at 8 and 10 days post-treatment, respectively.

Lethal concentration values (LC_{30} and LC_{50}) and 95% confidence intervals for DFB were calculated using probit analysis in POLO-Plus software (LeOra Software, Berkeley, CA, USA).

GPI exposure for gene expression analysis

For time-course gene expression analysis, synchronized third-instar larvae were exposed to 500 mg/L GPI (the highest concentration tested in bioassays) or solvent control (1% acetone + 0.1% Triton X-100) using the leaf-dip method described in Section 2.11.

Surviving larvae were collected at 24, 48, 72, and 96 h post-treatment. At each time point, three biological replicates (10 pooled larvae each) were flash-frozen in liquid nitrogen and stored at -80°C until RNA extraction. This sampling scheme ensured sufficient RNA yield while minimizing inter-individual variability.

Quantitative real-time PCR (RT-qPCR) analysis

Total RNA was extracted from frozen samples using RNAiso Plus reagent (TaKaRa, Kusatsu, Japan). RNA concentration and purity were assessed by NanoDrop 2000c spectrophotometer (Thermo Fisher Scientific). Only samples with A_{260}/A_{280} ratios between 1.9 and 2.1 and A_{260}/A_{230} ratios >1.8 were used for downstream analysis. RNA integrity was confirmed by agarose gel electrophoresis (sharp 28S/18S rRNA bands, ratio ≈ 2:1). cDNA was synthesized from 1 μg RNA using PrimeScript™ RT Reagent Kit with gDNA Eraser (TaKaRa).

Gene-specific primers for *PxGP*, *trehalase* (*PxTre*), *hexokinase* (*PxHex*), phosphoenolpyruvate carboxykinase (*PxPEPCK*), *PxG-6-Pase*, and the reference gene *PxRPS13* (ribosomal protein S13) were designed using Primer-BLAST (NCBI) and are listed in Table S1. *PxRPS13* was selected based on its stable expression across developmental stages and treatment conditions (geNorm M value < 0.5) [55]. All primers were validated for specificity (single peak in melt-curve), efficiency (90-110%, $R^2 > 0.98$), and absence of primer-dimers (no-template controls).

RT-qPCR reactions were performed on a QuantStudio™ 5 Real-Time PCR System (Thermo Fisher Scientific) using TB Green® Premix Ex Taq™ II (Tli RNaseH Plus) (2×) (TaKaRa) in 20 μL reactions. The thermal cycling conditions were as follows: initial denaturation at 95°C for 30 s; 40 cycles of 95°C for 15 s (denaturation) and 60°C for 30 s (annealing/extension); followed by melt-curve analysis. Each sample was analyzed in technical triplicate, and each biological replicate consisted of three independent samples. Relative gene expression was calculated using the $2^{-\Delta\Delta Ct}$ method [56].

RNA interference (RNAi)

A conserved 606 bp region of *PxGP* (nucleotides 66-671, part of the AMP-binding domain) was selected for RNAi. The fragment was amplified from larval cDNA using primers flanked by T7 promoters (Table S2). Double-stranded RNA (dsRNA) was synthesized with the T7 RiboMax™ Express RNAi System (Promega, Madison, WI, USA). The dsRNA of green fluorescent protein (ds*GFP*, 541 bp) was synthesized using a pGFP plasmid template as a non-specific negative control. Following synthesis, dsRNA was treated with RNase-free DNase I (30 min at 37°C), purified by isopropanol precipitation, and integrity verified by 1.5% agarose gel electrophoresis. Concentration and purity (A_{260}/A_{280}=1.9-2.1) was measured using a NanoDrop spectrophotometer. Purified dsRNA was resuspended in nuclease-free water at concentrations of 6,000, 10,000, or 14,000 ng/μL and stored in single-use aliquots at -80°C.

For microinjection, synchronized early third-instar larvae (6-12 h post-molt) were briefly chilled on ice for 2-3 min and injected laterally using a DMP-300 Injector (Micrology Precision Instruments, Ltd, Wuhan, China). After recovery on fresh cabbage leaves for 30 min at room temperature, larvae were maintained under standard rearing conditions. Phenotypic parameters (mortality, molting success, pupation rate, adult emergence) were monitored daily for 10 days. Larvae were collected at 24, 48, 72, and 96 h post-injection for RT-qPCR analysis to confirm target gene knockdown (n = 3 biological replicates, each containing 10 pooled larvae per time point).

Metabolite quantification

To directly assess metabolic flux alterations following Px*GP* knockdown, we quantified four key metabolites in the glycogen-glucose metabolic axis using commercial enzymatic assay kits: glycogen and glucose (Glycogen Assay Kit, Grace Biotechnology, Suzhou, China, Cat# G0590W96), trehalose (Trehalose Assay Kit, Grace Biotechnology, Cat# G0553W96), and glucose-6-phosphate (G6P Assay Kit, Beyotime Biotechnology, Shanghai, China, Cat# S0185). All kits utilize colorimetric or fluorometric enzymatic reactions and were performed according to the manufacturers' protocols with minor modifications as described below.

Third-instar larvae injected with ds*GP* (14,000 ng/μL, the highest dose achieving maximal knockdown) or ds*GFP* control were collected at 48, 72, and 96 h post-injection. At each time point, three biological replicates were collected, each consisting of 10 pooled larvae. Samples were immediately flash-frozen in liquid nitrogen and stored at -80°C until analysis.

For metabolite extraction, frozen larvae were homogenized on ice in ice-cold extraction buffer specific to each metabolite assay (typically 100 μL buffer per 10 mg tissue). For glycogen extraction, samples were homogenized in deionized water and immediately boiled for 3 min to inactivate endogenous glycogenolytic enzymes. For trehalose, glucose, and G6P extraction, samples were homogenized in the respective assay buffers provided in the kits. Homogenates were centrifuged at 12,000 × g for 10 min at 4°C, and supernatants were immediately used for metabolite quantification or stored at -80°C for no more than 24 h.

Metabolite quantification was performed in 96-well microplates using Infinite 200 PRO microplate reader (Tecan, Männedorf, Switzerland) at the wavelengths specified in each kit's protocol. Sample metabolite concentrations were calculated by comparison with the absorbance of the kit's standard. Metabolite concentrations were normalized to tissue protein content to account for variation in tissue input. Protein concentration in the crude lysates was determined using the Protein Quantification Kit (BCA Assay) (Abbkine Scientific) with bovine serum albumin as the standard. All samples were analyzed in technical triplicate. Final metabolite levels were expressed as: Glycogen: mg/mg protein; Glucose: μmol/mg protein; Trehalose: μmol/mg protein; G6P: μmo/mg protein.

Data are presented as mean ± standard error of the mean (SEM). Statistical significance between ds*GP* and ds*GFP* groups at different time point was assessed using two-way ANOVA (GraphPad Prism 8.0), with Sidak's multiple comparisons test [57]. Statistical significance was set at $P < 0.05$ (*), $P < 0.01$ (**) or $P < 0.001$ (***).

Data availability

All data generated or analyzed during this study arewithin the paper and its Supporting information file; source data files have been provided for all figures.

Supplementary Figures and Tables

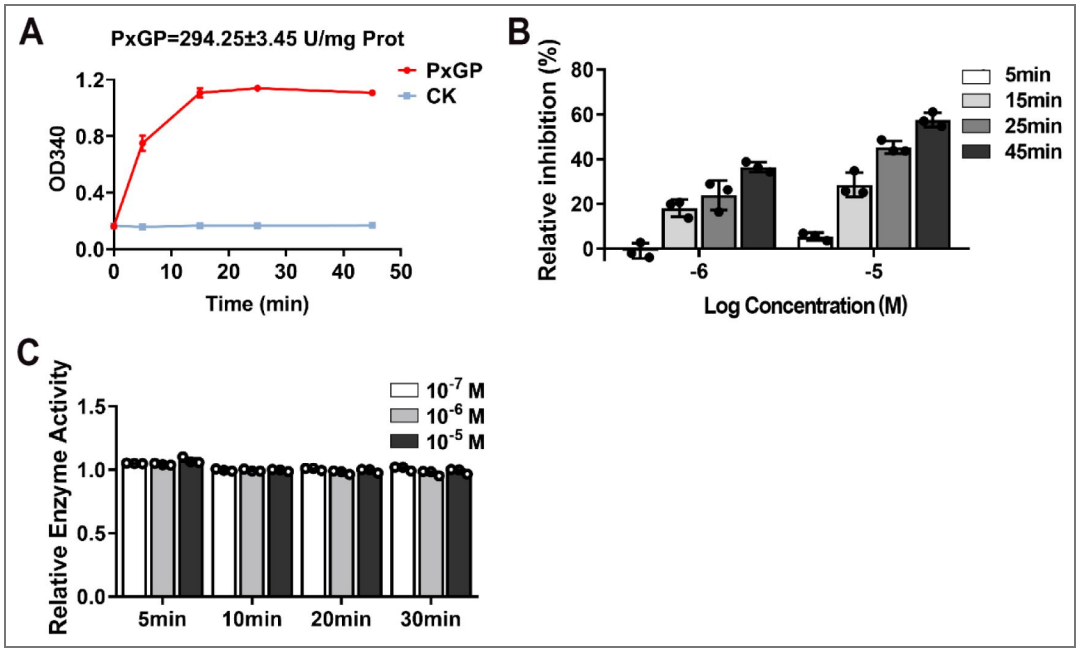

Figure S1. Enzymatic activity of purified PxGP and inhibition assays using crude larval lysate. (A) Reaction kinetics of purified, activated PxGP-a (red line) compared to a no-enzyme control (CK, blue line). The specific activity was calculated to be 294.25 ± 3.45 U/mg Prot (mean ± SEM). (B) Inhibition of native GP activity in a crude larval lysate by GPI. Activity was measured at 5, 15, 25, and 45 min post-incubation. (C) Effect of DFB on native GP activity in a crude larval lysate. DFB showed no significant inhibition at any concentration or time point. Data in (B) and (C) are presented as mean ± SEM (n = 3).

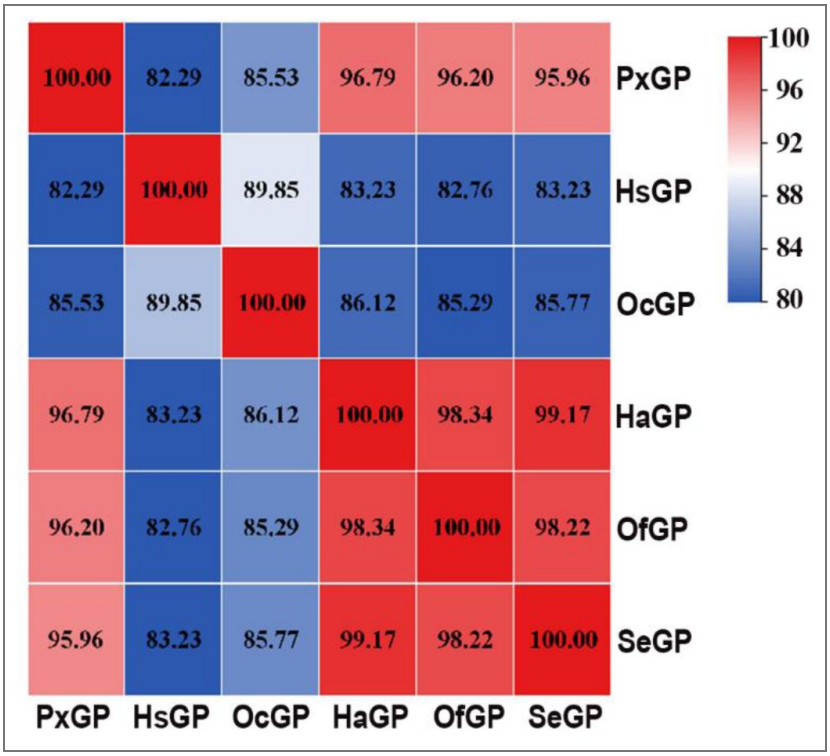

Figure S2. Heatmap depicting pairwise sequence similarity of glycogen phosphorylase among six species.

The heatmap displays the percentage of global sequence similarity calculated from pairwise alignments using TBtools. The six species (*Plutella xylostella*, *Homo sapiens*, *Oryctolagus cuniculus*, *Helicoverpa armigera*, *Ostrinia furnacalis* and *Spodoptera exigua*) are arranged in the same order along both axes. The color intensity in each cell corresponds to the similarity percentage, as shown in the color key (from blue—low, to red—high). Numerical values are shown within the cells.

Table S1. **Primer sequences used in this study.**

Primer Name	Sequence (5'-3')	Amplicon (bp)	Efficiency (%)	R^2
RT-qPCR				
qPxGP-F	ACCCCAACGACCACTTCTTC	170	107.86	0.986
qPxGP-R	CGACCTTCTCAGGGAGGCTA			
qPxTre-F	GCTCTACAACGACTCCAAG	139	105.35	0.997
qPxTre-R	CTGCGACACGAACTCCT			
qPxHEX-F	CTGGGATTCACATTCAGTTT	136	90.27	0.994
qPxHEX-R	TGGCAATAGCGTCTTTCA			
qPxpepck-F	TGTCAACTGGTTCCGCAAGAATG	160	102.08	0.996
qPxpepck-R	TGTGTTCAAGCAGCCGTCTCT			
qG-6-P-F	GAGTTACTGCTGATTGTGATGTGGAT	200	98.17	0.995
qG-6-P-F	AGGGCTGGTGCTAGGAATGC			
qPRS13-F	TCAGGCTTATTCTCGTCG	123	91.22	0.99
qPRS13-R	GCTGTGCTGGATTCGTAC			
dsRNA Synthesis				
dsPxGP-F	CGCCGCTACAAGTCATCC			
dsPxGP-R	CCTTCCTCCTCAATCAACGA			
dsT7PxGP-F	taatacgactcactatagggCGCCGCTACAAGTCATCC			
dsT7PxGP-R	taatacgactcactatagggCCTTCCTCCTCAATCAACGA			
dsGFP-F	GAGAAGAACTTTTCACTGCA			
dsGFP-R	TGTTGATAATGGTCTGCTAG			
dsT7GFP-F	taatacgactcactatagggGAGAAGAACTTTTCACTGCA			
dsT7GFP-R	taatacgactcactatagggTGTTGATAATGGTCTGCTAG			
Protein expression				
pFastbac-F	TATTCCGGATTATTCATACC			

Table S1. (continued)

pFastbac-R	ACAAATGTGGTATGGCTGA
pUC/M13-F	CCCAGTCACGACGTTGTAAAACG
pUC/M13-R	AGCGGATAACAATTTCACACAGG

Note: Lowercase represents the T7 promoter sequence: taatacgactcactataggg.

The qPCR amplification efficiency is represented by Efficiency (%).

Table S2. Toxicity of Diflubenzuron (DFB) against 3rd-instar *Plutella xylostella* larvae at 120 h.

toxicity regression equation	LC_{30} (mg/L) (95% CI)	LC_{50} (mg/L) (95% CI)	χ^2	*P*
y=-5.927+2.511x	141.900 (67.893-206.576)	229.537 (145.287-331.784)	11.946	0.683

Additional information

Author contribution

Conceptualization: Zhen Tian, Yalin Zhang and Jiyuan Liu.

Data curation: Yifei Zhou, Yanqi Kang, and Yan Liu.

Formal analysis: Yifei Zhou.

Funding acquisition: Zhen Tian, Yalin Zhang and Jiyuan Liu.

Investigation: Yifei Zhou, Yanqi Kang, Yan Liu, Ruichi Li, Dongliang Wang, Chong Yi, Yifan Li, Yalin Zhang, Zhen Tian, and Jiyuan Liu.

Methodology: Yifei Zhou, Yanqi Kang, Yifan Li, and Jiyuan Liu.

Resources: Jiyuan Liu, Zhen Tian, and Yalin Zhang.

Supervision: Jiyuan Liu, Zhen Tian, and Yalin Zhang.

Validation: Yifei Zhou, Yanqi Kang, Yan Liu, and Jiyuan Liu.

Visualization: Yifei Zhou, Zhen Tian, and Jiyuan Liu.

Writing – original draft: Yifei Zhou.

Writing–review & editing: Yifei Zhou, Zhen Tian, and Jiyuan Liu.

Funding

This research was supported by the Guangdong Basic and Applied Basic Research Foundation (*https://gdstc.gd.gov.cn/*) grant 2024A1515010156 (to JYL), the National Natural Science Foundation of China (*https://www.nsfc.gov.cn/*) grants 32172452 (to JYL) and 32372626 (to ZT), the Shenzhen Basic Research Program (*https://stic.sz.gov.cn/*) grant JCYJ20240813152006009 (to JYL), and Chinese Universities Scientific Fund (*https://www.nwafu.edu.cn/*) grants 2452022348 (to YLZ), 2452021151 (to YLZ).

Funding

Funder	Grant reference number	Author
GDSTC | Basic and Applied Basic Research Foundation of Guangdong Province	2024A1515010156	Jiyuan Liu
National Natural Science Foundation of China (NSFC)	32172452	Jiyuan Liu
MOST | National Natural Science Foundation of China (NSFC)	32372626	Zhen Tian
Shenzhen Municipal Fundamental Research Program	JCYJ20240813152006009	Jiyuan Liu
MOE | Chinese Universities Scientific Fund	2452022348	Yalin Zhang
MOE | Chinese Universities Scientific Fund	2452021151	Yalin Zhang

Author ORCID iDs

Jiyuan Liu: https://orcid.org/0000-0002-3524-2064

Additional files

Supplementary Data S1. Contains values used for data presentation of Figures 2-4, 6-9, and S1.

References

1. **Van Leeuwen T,** Demaeght P, Osborne EJ, Dermauw W, Gohlke S, Nauen R, et al. (2012) Population bulk segregant mapping uncovers resistance mutations and the mode of action of a chitin synthesis inhibitor in arthropods. *Proc Natl Acad Sci U S A* **109**:4407-12 https://doi.org/10.1073/pnas.1200068109 | PubMed
2. **Ishaaya I,** Casida JE., Dietary TH (1974) 6040 alters composition and enzyme activity of housefly larval cuticle. *Pestic Biochem Physiol* **4**:484-90 https://doi.org/10.1016/0048-3575(74)90073-X
3. **Post LC,** de Jong BJ, Vincent WR (1974) 1-(2,6-disubstituted benzoyl)-3-phenylurea insecticides: Inhibitors of chitin synthesis. *Pestic Biochem Physiol* **4**:473-83 https://doi.org/10.1016/0048-3575(74)90072-8
4. **Suzuki Y,** Shiotsuki T, Jouraku A, Miura K, Minakuchi C (2017) Benzoylurea resistance in western flower thrips *Frankliniella occidentalis* (Thysanoptera: Thripidae): the presence of a point mutation in chitin synthase 1. *J Pestic Sci* **42**:93-6 https://doi.org/10.1584/jpestics.D17-023 | PubMed
5. **Douris V,** Steinbach D, Panteleri R, Livadaras I, Pickett JA, Van Leeuwen T, et al. (2016) Resistance mutation conserved between insects and mites unravels the benzoylurea insecticide mode of action on chitin biosynthesis. *Proc Natl Acad Sci U S A* **113**:14692-7 https://doi.org/10.1073/pnas.1618258113 | PubMed
6. **Deul DH,** de Jong BJ, Kortenbach JAM (1978) Inhibition of chitin synthesis by two 1-(2,6-disubstituted benzoyl)-3-phenylurea insecticides. II. *Pestic Biochem Physiol* **8**:98-105 https://doi.org/10.1016/0048-3575(78)90096-2
7. **Nakagawa Y,** Matsumura F, Hashino Y (1993) Effect of diflubenzuron on incorporation of [^{3}H]-N-acetylglucosamine ([^{3}H]NAGA) into chitin in the intact integument from the newly molted American cockroach *Periplaneta americana*. Comp Biochem Physiol, Part C:Pharmacol. *Toxicol Endocrinol* **106**:711-5 https://doi.org/10.1016/0742-8413(93)90231-9 | PubMed
8. **Zimoch L,** Hogenkamp DG, Kramer KJ, Muthukrishnan S, Merzendorfer H (2005) Regulation of chitin synthesis in the larval midgut of *Manduca sexta*. *Insect Biochem Mol Biol* **35**:515-27 https://doi.org/10.1016/j.ibmb.2005.01.008 | PubMed
9. **Sun R,** Liu C, Zhang H, Wang Q (2015) Benzoylurea chitin synthesis inhibitors. *J Agric Food Chem* **63**:6847-65 https://doi.org/10.1021/acs.jafc.5b02460 | PubMed
10. **Baker DJ,** Timmons JA, Greenhaff PL (2005) Glycogen phosphorylase inhibition in type 2 diabetes therapy: a systematic evaluation of metabolic and functional effects in rat skeletal muscle. *Diabetes* **54**:2453-9 https://doi.org/10.2337/diabetes.54.8.2453 | PubMed
11. **Klabunde T,** Wendt KU, Kadereit D, Brachvogel V, Burger H-J, Herling AW, et al. (2005) Acyl ureas as human liver glycogen phosphorylase inhibitors for the treatment of type 2 diabetes. *J Med Chem* **48**:6178-93 https://doi.org/10.1021/jm049034y | PubMed
12. **Becker A,** Schlöder P, Steele JE, Wegener G (1996) The regulation of trehalose metabolism in insects. *Experientia* **52**:433-9 https://doi.org/10.1007/BF01919312 | PubMed
13. **Steele JE** (1982) Glycogen phosphorylase in insects. *Insect Biochemistry* **12**:131-47 https://doi.org/10.1016/0020-1790(82)90001-4
14. **Chen C-P,** Denlinger DL (1990) Activation of phosphorylase in response to cold and heat stress in the flesh fly, *Sarcophaga crassipalpis*. *J Insect Physiol* **36**:549-53 https://doi.org/10.1016/0022-1910(90)90022-8
15. **Joanisse DR,** Storey KB (1994) Enzyme activity profiles in an overwintering population of freeze-tolerant larvae of the gall fly, *Eurosta solidaginis*. J Comp Physiol. *B* **164**:247-55 https://doi.org/10.1007/BF00354086
16. **Cori CF,** Cori GT (1936) Mechanism of formation of hexosemonophosphate in muscle and isolation of a new phosphate ester. *Proc Soc Exp Biol Med* **34**:702-5 https://doi.org/10.3181/00379727-34-8759P

17. **Yamashita O,** Suzuki K, Hasegawa K (1975) Glycogen phosphorylase activity in relation to diapause initiation in Bombyx eggs. *Insect Biochem* **5**:707-18 https://doi.org/10.1016/0020-1790(75)90015-3

18. **Bornhorst JA,** Falke JJ (2000) Purification of proteins using polyhistidine affinity tags. *Methods Enzymol* **326**:245-54 https://doi.org/10.1016/s0076-6879(00)26058-8 | PubMed

19. **Oikonomakos NG** (2002) Glycogen phosphorylase as a molecular target for type 2 diabetes therapy. *Curr Protein Pept Sci* **3**:561-86 https://doi.org/10.2174/1389203023380422 | PubMed

20. **Rath VL,** Ammirati M, LeMotte PK, Fennell KF, Mansour MN, Danley DE, et al. (2000) Activation of human liver glycogen phosphorylase by alteration of the secondary structure and packing of the catalytic core. *Molecular Cell* **6**:139-48 https://doi.org/10.1016/S1097-2765(05)00006-7 | PubMed

21. **Muthukrishnan S,** Merzendorfer H, Arakane Y, Kramer KJ (2012) 7 - Chitin metabolism in insects. In: Gilbert LI (Ed). *Insect Molecular Biology and Biochemistry* San Diego: Academic Press. pp. 193-235

22. **Hudson JW,** Golding GB, Crerar MM (1993) Evolution of allosteric control in glycogen phosphorylase. *J Mol Biol* **234**:700-21 https://doi.org/10.1006/jmbi.1993.1621 | PubMed

23. **Li Y,** Yao Y, Zhao Y, Di Y, Zhao X (2021) The steroid hormone 20-hydroxyecdysone counteracts insulin signaling *via* insulin receptor dephosphorylation. *J Biol Chem* **296** https://doi.org/10.1016/j.jbc.2021.100318 | PubMed

24. **Uryu O,** Kamae Y, Tomioka K, Yoshii T (2013) Long-term effect of systemic RNA interference on circadian clock genes in hemimetabolous insects. *J Insect Physiol* **59**:494-9 https://doi.org/10.1016/j.jinsphys.2013.02.009 | PubMed

25. **Denlinger DL,** Yocum GD, Rinehart JP. (2012) 10 - Hormonal control of diapause. In: Gilbert LI (Ed). *Insect Endocrinology* San Diego: Academic Press. pp. 430-63 https://doi.org/10.1016/b978-0-12-384749-2.10010-x

26. **Shakeel M,** Du J, Li S, Zhou Y, Sarwar N, Bukhari SA (2020) Characterization, knockdown and parental effect of hexokinase gene of *Cnaphalocrocis medinalis* (Lepidoptera: Pyralidae) revealed by RNA interference. *Genes* **11**:1258 https://doi.org/10.3390/genes11111258 | PubMed

27. **Martins da Silva R,** de Oliveira Daumas Filho CR, Calixto C, Nascimento da Silva J, Lopes C, da Silva Vaz I, et al. (2023) PEPCK and glucose metabolism homeostasis in arthropods. Insect Biochem Mol Biol. *Insect biochemistry and molecular biology* **160** https://doi.org/10.1016/j.ibmb.2023.103986 | PubMed

28. **Miyamoto T,** Amrein H (2017) Gluconeogenesis: An ancient biochemical pathway with a new twist. *Fly* **11**:218-23 https://doi.org/10.1080/19336934.2017.1283081 | PubMed

29. **Arrese EL,** Soulages JL (2010) Insect fat body: energy, metabolism, and regulation. *Annu Rev Entomol* **55**:207-25 https://doi.org/10.1146/annurev-ento-112408-085356 | PubMed

30. **Moreira DC,** Hermes-Lima M (2024) Dynamics of redox metabolism during complete metamorphosis of insects: Insights from the sunflower caterpillar *Chlosyne lacinia* (Lepidoptera). *Antioxidants* **13**:959 https://doi.org/10.3390/antiox13080959 | PubMed

31. **Nelson DL,** Cox MM. (2017) *Regulation of metabolic pathways Lehninger Principles of Biochemistry* New York: W. H. Freeman and Company. pp. 496-509

32. **Wang X,** Huang Z, Li Y, Jin K, Dong D, Wang J, et al. (2022) Krüppel-like factor 15 integrated autophagy and gluconeogenesis to maintain glucose homeostasis under 20-hydroxyecdysone regulation. *PLoS Genet* **18**:e1010229 https://doi.org/10.1371/journal.pgen.1010229 | PubMed

33. **Chippendale GM** (1973) Diapause of the southwestern corn borer, *Diatraea grandiosella*: utilization of fat body and haemolymph reserves. *Entomol Exp Appl* **16**:395-406 https://doi.org/10.1111/j.1570-7458.1973.tb00289.x

34. **Terra WR,** Ferreira C (1994) Insect digestive enzymes: properties, compartmentalization and function. *Comp Biochem Physiol, Part B:Biochem Mol Biol* **109**:1-62 https://doi.org/10.1016/0305-0491(94)90141-4

35. **Sorkhabi-Abdolmaleki S,** Zibaee A, Hoda H, Fazeli-Dinan M (2014) Purification and characterization of midgut α-amylase in a predatory bug, *Andralus spinidens*. *J Insect Sci* **14** https://doi.org/10.1093/jis/14.1.65 | PubMed

36. **Huynh N,** Ou Q, Cox P, Lill R, King-Jones K (2019) Glycogen branching enzyme controls cellular iron homeostasis via Iron Regulatory Protein 1 and mitoNEET. *Nat Commun* **10**:5463 https://doi.org/10.1038/s41467-019-13237-8 | PubMed

37. **Nestel D,** Tolmasky D, Rabossi A, Quesada-Allué LA (2003) Lipid, carbohydrates and protein patterns during metamorphosis of the mediterranean fruit fly, *Ceratitis capitata* (Diptera: Tephritidae). *Ann Entomol Soc Am* **96**:237-44 https://doi.org/10.1603/0013-8746(2003)096[0237:LCAPPD]2.0.CO;2

38. **Ghani MU,** Yang Z, Feng T, Chen J, Khosravi Z, Wu Q, et al. (2024) Comprehensive review on glucose 6 phosphate dehydrogenase: A critical immunometabolic and redox switch in insects. *Int J Biol Macromol* **273**:132867 https://doi.org/10.1016/j.ijbiomac.2024.132867 | PubMed

39. **Cohen E** (2001) Chitin synthesis and inhibition: a revisit. *Pest Manage Sci* **57**:946-50 https://doi.org/10.1002/ps.363 | PubMed

40. **Merzendorfer H** (2006) Insect chitin synthases: a review. J Comp Physiol. *B* **176**:1-15 https://doi.org/10.1007/s00360-005-0005-3 | PubMed

41. **Li S,** Yu X, Feng Q (2019) Fat body biology in the last decade. *Annu Rev Entomol* **64**:315-33 https://doi.org/10.1146/annurev-ento-011118-112007 | PubMed

42. **Zhang N,** Meng X, Jiang H, Ge H, Zheng Y, Qian K, et al. (2022) Metabolic and transcriptional responses to starvation are regulated by FOXO in the red flour beetle, *Tribolium castaneum*. *Physiol Entomol* **47**:209-18 https://doi.org/10.1111/phen.12390

43. **Luo YJ,** Chen Y, Wang XJ, Wang ST, Yang YY, Xu HX, et al. (2022) Validamycin affects the development and chitin metabolism in Spodoptera frugiperda by inhibiting trehalase activity. *Entomologia Generalis* **42**:931-9 https://doi.org/10.1127/entomologia/2022/1608

44. **Shao ZM,** Ding JH, Jiang DL, Liu ZX, Li YJ, Wang J, et al. (2021) Characterization and functional analysis of trehalase related to chitin metabolism in *Glyphodes pyloalis* walker (Lepidoptera: Pyralidae). *Insects* **12**:370 https://doi.org/10.3390/insects12040370 | PubMed

45. **Sheng X,** Wang MM, Zhang GD, Su Y, Fang HB, Yu ZH, et al. (2024) Dual inhibition of oxidative phosphorylation and glycolysis to enhance cancer therapy. *Bioorg Chem* **147** https://doi.org/10.1016/j.bioorg.2024.107325 | PubMed

46. **Aisu Y,** Oshima N, Hyodo F, Elhelaly AE, Masuo A, Okada T, et al. (2024) Dual inhibition of oxidative phosphorylation and glycolysis exerts a synergistic antitumor effect on colorectal and gastric cancer by creating energy depletion and preventing metabolic switch. *PLoS One* **19**:e0309700 https://doi.org/10.1371/journal.pone.0309700 | PubMed

47. **Adedeji EO,** Ogunlana OO, Fatumo S, Aromolaran OT, Beder T, Koenig R, et al. (2023) The central metabolism model of anopheles gambiae: A tool for understanding malaria vector biology. In: Isibor PO, Akinduti P, Oranusi SU, Popoola JO (Eds). *Biotechnological approaches to sustainable development goals* Cham: Springer Nature Switzerland.

48. **Germing K,** Navarrete CAD, Schiermeyer A, Hommen U, Zühl L, Eilebrecht S, et al. (2025) Crop protection by RNA interference: a review of recent approaches, current state of developments and use as of 2013. *Environ Sci Eur* **37**:15 https://doi.org/10.1186/s12302-025-01052-6

49. **Imran M,** Feng X, Sun Z, Al Omari H, Zhang G, Zhu J, et al. (2025) Nanotechnology-driven gene silencing: advancements in SIGS–dsRNA technology for sustainable disease management. *Chem Biol Technol Agric* **12**:31 https://doi.org/10.1186/s40538-025-00738-6

50. **Sharma Y,** Padha S, Dhar A, Baweja V, Singh IK (2023) RNAi-based biopesticides: A review of recent studies in Lepidopteran insects. *Proc Zool Soc* **76**:373-81 https://doi.org/10.1007/s12595-023-00489-y

51. **Jang C,** Chen L, Rabinowitz JD. (2018) Metabolomics and Isotope tracing. *Cell* **173**:822-37 https://doi.org/10.1016/j.cell.2018.03.055 | PubMed

52. **Chen C,** Wu Y, Li J, Wang X, Zeng Z, Xu J, et al. (2023) TBtools-II: A "one for all, all for one" bioinformatics platform for biological big-data mining. *Mol Plant* **16**:1733-42 https://doi.org/10.1016/j.molp.2023.09.010 | PubMed

53. **Shelton AM,** Robertson JL, Tang JD, Perez C, Eigenbrode SD, Preisler HK, et al. (1993) Resistance of diamondback moth (Lepidoptera: Plutellidae) to *Bacillus thuringiensis* subspecies in the field. *J Econ Entomol* **86**:697-705 https://doi.org/10.1093/jee/86.3.697

54. **Abbott WS** (1925) A method of computing the effectiveness of an insecticide. *Journal of Economic Entomology* **18**:265-7 https://doi.org/10.1093/jee/18.2.265a

55. **Fu W,** Xie W, Zhang Z, Wang S, Wu Q, Liu Y, et al. (2013) Exploring valid reference genes for quantitative real-time PCR analysis in *Plutella xylostella* (Lepidoptera: Plutellidae). *Int J Biol Sci* **9**:792-802 https://doi.org/10.7150/ijbs.5862 | PubMed

56. **Livak KJ,** Schmittgen TD (2001) Analysis of relative gene expression data using real-tme quantitative PCR and the $2^{-\Delta\Delta CT}$ method. *Methods* **25**:402-8 https://doi.org/10.1006/meth.2001.1262 | PubMed

57. **Abdi H.** (2007) The Bonferonni and Šidák corrections for multiple comparisons. In: Salkind N (Ed). *Encyclopedia of measurement and statistics* Thousand Oaks: SAGE. pp. 103-6

Yifei Zhou, Yanqi Kang, Yan Liu, Ruichi Li, Dongliang Wang, Chong Yi, Yifan Li, Yalin Zhang, Zhen Tian, Jiyuan Liu (2026) Metabolic compensation via gluconeogenesis explains the non-essentiality of glycogen phosphorylase as an insecticidal target in Plutella xylostella. Mendeley Data. https://doi.org/10.17632/w6bzpb32vz.1

Reference Sequence NCBI (2022) Plutella xylostella glycogen phosphorylase (LOC105390085), mRNA. NCBI Nucleotide. ID XM_038119125.2 https://www.ncbi.nlm.nih.gov/nuccore/XM_038119125.2

Peer reviews

Reviewer #1 (Public review):

Summary:

In this study, the authors investigate whether glycogen phosphorylase is a potential molecular target of benzoylphenylurea insecticides and examine the physiological consequences of inhibiting glycogen breakdown in the diamondback moth Plutella xylostella. The authors express and characterize recombinant glycogen phosphorylase, test its inhibition by a mammalian glycogen phosphorylase inhibitor and by the insecticide diflubenzuron, and assess the physiological effects of glycogen phosphorylase inhibition through chemical exposure and RNA interference. Based on these experiments, the authors conclude that benzoylphenylurea insecticides do not target glycogen phosphorylase and propose that insects compensate for glycogen phosphorylase inhibition through activation of gluconeogenesis, allowing them to maintain glucose homeostasis and complete development despite strong suppression of the enzyme.

Strengths:

The study addresses an interesting and long-standing question in insect toxicology regarding the mechanism of action of benzoylphenylurea insecticides. The authors combine several complementary approaches, including recombinant enzyme characterization, inhibitor assays, RNA interference, gene expression analyses, and metabolite measurements. The biochemical characterization of the recombinant glycogen phosphorylase and the demonstration that the tested glycogen phosphorylase inhibitor can strongly inhibit enzyme activity represent important technical strengths. In addition, the study integrates biochemical and physiological observations to explore how insects might compensate for disruptions in central carbohydrate metabolism.

Weaknesses:

Several aspects of the central conclusions rely on indirect evidence and would benefit from additional validation. The proposed compensatory mechanism (gluconeogenesis supported

by amino acid mobilization) is inferred primarily from transcriptional changes in gluconeogenic genes, reduced protein levels, and changes in metabolite concentrations. While these observations are consistent with increased gluconeogenic activity, they do not directly demonstrate metabolic flux through this pathway. Direct measurements of gluconeogenic flux would be required to confirm that carbon derived from non-carbohydrate substrates contributes to glucose production.

Some interpretations are also speculative. For example, the lack of glycogen accumulation following glycogen phosphorylase knockdown is attributed to alternative glycogen degradation pathways, such as α-amylase or glycogen debranching enzymes, but these possibilities are not experimentally examined. Measuring the expression or activity of these enzymes would help evaluate whether such pathways contribute to the observed metabolic response.

The physiological consequences of the proposed metabolic compensation are also not fully explored. If proteins are mobilized to support gluconeogenesis, this shift might be expected to affect organismal traits such as adult body size, flight capacity, or reproductive performance. Assessing these traits could provide valuable insight into whether the proposed compensatory metabolism carries fitness costs.

Finally, some conclusions extend beyond the direct evidence presented. The study shows that diflubenzuron does not inhibit glycogen phosphorylase in vitro, but broader conclusions regarding the mechanism of action of benzoylphenylurea insecticides as a class may require additional evidence. In addition, some biochemical and cell-based observations would benefit from confirmation in whole insects, given that metabolic regulation can differ substantially between isolated enzyme or cell-based systems and intact larvae, where hormonal signaling, tissue interactions, and nutrient availability influence metabolic responses.

https://doi.org/10.7554/eLife.111144.1.sa2

Reviewer #2 (Public review):

(1) Significance of the findings and strength of the evidence

This manuscript evaluates the hypothesis that benzoylurea (BPU) insecticides exert their effects through inhibition of glycogen phosphorylase rather than chitin synthase (CHS). The central premise-that structural similarity among acylurea compounds implies shared molecular targets-is not supported by existing evidence.

Extensive genetic and biochemical studies, including Reference 5, demonstrate that chitin synthase is the primary insecticidal target of BPUs. In particular, amino acid substitutions at a single site in CHS confer high levels of resistance to diflubenzuron and related compounds, with causality established through CRISPR/Cas9 editing in Drosophila melanogaster. This body of evidence substantially weakens the rationale for proposing glycogen phosphorylase as an alternative primary target.

The manuscript reports that an acylurea compound previously identified as an inhibitor of mammalian glycogen phosphorylase also inhibits glycogen phosphorylase from Plutella xylostella, while diflubenzuron does not. This observation is consistent with prior work showing that glycogen phosphorylase inhibition among acylureas depends on specific side chain substitutions rather than the shared acylurea core. Consequently, the finding does not support the broader inference that acylurea structure predicts common biological function.

The manuscript further argues that inhibition of glycogen phosphorylase is not insecticidal and attributes this to metabolic compensation through alternative glucose producing pathways. While it is well established that eukaryotic cells possess multiple mechanisms for

maintaining glucose availability, the evidence provided here does not fully support the broader claim that this mechanism explains the lack of insecticidal activity. In particular, the conclusion that the study "resolves" the primary hypothesis is not justified by the data presented.

Overall, while some experimental observations are sound in isolation, the overarching conclusions are not supported by the strength of the evidence. The significance of the findings is therefore limited.

(2) Interpretation in the context of existing literature

The introduction states that the molecular target of BPU insecticides remains a major unresolved controversy. However, multiple prior studies, including References 1, 4, and 5, provide strong genetic evidence that CHS is the primary and essential target of BPUs. These results demonstrate causality rather than simple correlation, particularly through targeted gene editing approaches.

The manuscript further claims that biochemical studies have failed to demonstrate CHS inhibition by BPUs in cell free assays. However, the cited references (6-9) did not express CHS in such assays and therefore do not directly address this question. As a result, the suggested discrepancy between genetic and enzymatic evidence is not well founded.

Structural analysis of acylurea compounds indicates that biological activity depends on side chain composition rather than the conserved acylurea core. Prior screening studies (Reference 11) show substantial variability in glycogen phosphorylase inhibition among acylureas despite a shared core structure. This undermines the proposal that the acylurea moiety itself constitutes a meaningful clue to a shared molecular mechanism.

Regarding implications for pesticide design, targeting chitin synthesis remains an attractive strategy because chitin is essential for arthropods and absent in mammals, providing both efficacy and specificity. By contrast, metabolic enzymes such as glycogen phosphorylase are widely conserved, making them less suitable targets from a toxicological and safety perspective.

(3) Specific technical comments

The manuscript uses the term "dataology," which is neither defined nor contextualized within the text. As currently used, the term appears unrelated to the subject matter and may be confusing to readers. Clarification or removal would improve clarity.

https://doi.org/10.7554/eLife.111144.1.sa1

Author response:

> ***Public Reviews:***
>
> ***Reviewer #1 (Public review):***
>
> *(1) The proposed compensatory mechanism is inferred primarily from transcriptional changes and metabolite levels; direct measurements of gluconeogenic flux are lacking.*

We agree that isotopic tracer experiments would provide the most direct evidence for gluconeogenic flux. While such experiments are beyond the scope of the current revision, we will explicitly acknowledge this as a key limitation and clearly state it as an important direction for future research. We note, however, that the convergent evidence from multiple independent lines, transcriptional upregulation of PEPCK and G-6-Pase, declining protein levels, altered amino acid profiles, and maintained trehalose levels, collectively supports gluconeogenic activation, even though each individual line is indirect. In the revised

manuscript, we will present this evidence more cautiously, framing it as "consistent with gluconeogenic compensation" rather than definitively establishing metabolic flux.

> *(2) Alternative glycogen degradation pathways (α-amylase, glycogen debranching enzymes) are proposed but not experimentally examined.*

We have now directly addressed this by measuring, via RT-qPCR, the expression of glycogen branching enzyme (*GBE*) and *α-amylase* following *PxGP* knockdown. Our preliminary results reveal a striking and informative pattern:

GBE was significantly upregulated at 24 h (+29.24%), 48 h (+16.78%), and 96 h (+44.46%) post-injection, indicating transcriptional activation of an alternative glycogen-metabolizing enzyme in response to GP suppression.

α-Amylase showed no significant change at any time point, suggesting that the compensatory response is pathway-specific rather than a generalized upregulation of all starch/glycogen-degrading enzymes.

This differential response, *GBE* up while *α-amylase* unchanged, provides the first direct evidence that *P. xylostella* selectively activates specific alternative glycogen catabolic pathways when GP function is compromised. These data will be incorporated into the revised manuscript as a new figure panel.

> *(3) Physiological consequences of the proposed metabolic compensation (fitness costs) are not explored.*

We have now assessed fitness consequences of *PxGP* knockdown by measuring feeding rate, larval body weight, and pupal weight. The results reveal a transient but significant fitness cost:

Feeding rate: no significant difference between ds*GP* and ds*GFP* groups across all time points (24–120 h), indicating that the observed metabolic changes are not attributable to reduced food intake.

Larval weight: significantly reduced at 24 h (−29.10%) and 48 h (−25.38%) in the ds*GP* group, demonstrating that metabolic compensation carries a measurable short-term cost.

Pupal weight: no significant difference, indicating that larvae recover from the transient weight deficit before pupation.

This pattern, transient larval weight loss with full pupal recovery, is consistent with our proposed model: GP suppression triggers protein catabolism to fuel gluconeogenesis (explaining the weight loss), but the compensatory mechanism is sufficiently effective to restore metabolic homeostasis before the pupal transition. Adult wing area and female fecundity measurements are currently in progress and will be included in the revised manuscript.

> *(4) Enzyme activity is not measured in RNAi-treated insects; only transcript-level knockdown is reported.*

We have now measured GP enzyme activity (GPa) in crude extracts from RNAi-treated larvae using the coupled-enzyme spectrophotometric assay. The results provide important new insights:

Per-larva GP activity was significantly reduced at 24 h (−27.57%) and 48 h (−29.28%), confirming that RNAi-mediated transcript suppression translates to reduced enzyme function *in vivo*.

Per-protein GP activity showed a significant reduction only at 48 h (−10.35%). This apparent discrepancy is explained by a substantial decrease in total protein concentration at 24 h (−44.48%), which then gradually recovered. When enzyme activity is normalized to a declining protein pool, the per-protein reduction appears smaller.

Importantly, the 44.48% decline in total protein at 24 h provides independent biochemical confirmation of our proposed protein catabolism: it is consistent with the mobilization of protein stores to supply amino acids for gluconeogenesis, directly supporting the compensatory mechanism described in our manuscript.

These enzyme activity data will be presented alongside the existing transcript-level data in the revised manuscript, providing a complete picture from gene expression through enzyme function.

> *(5) Conclusions regarding BPU class may require testing additional compounds beyond diflubenzuron.*

We agree and will explicitly limit our conclusion to diflubenzuron in the revised manuscript. The relevant text will be revised to state that "DFB does not inhibit PxGP" rather than making broader claims about the BPU class as a whole.

> *(6) Structural evidence that GPI can bind PxGP in a comparable manner to its mammalian target is lacking.*

We have performed molecular docking and binding free energy analysis to address this concern directly. The PxGP homodimer structure was modeled using SWISS-MODEL with the rabbit muscle GP–acyl urea co-crystal structure (PDB: 2ATI; Klabunde et al., 2005) as the template. Molecular docking and MM/GBSA calculations were performed using Cresset Flare V11.

Key findings:

GPI exhibited substantially stronger binding to PxGP (ΔG = −34.63 kcal/mol) compared to DFB (ΔG = −29.29 kcal/mol), with a ΔΔG of −5.34 kcal/mol.

Energy decomposition revealed that van der Waals interactions are the primary driver of selectivity (ΔG_{VDW} = −11.49 kcal/mol), reflecting superior shape complementarity of GPI within the binding pocket.

GPI was predicted to bind at the allosteric site at the dimer interface, engaging seven residues across both subunits (Asn44 and Val45 from chain A; Trp67, Gln71, Tyr75, Arg193, and Asp227 from chain B), a binding mode consistent with the experimentally determined site of acyl urea inhibitors in mammalian GP.

DFB contacted only six residues, primarily from a single subunit, and its difluorobenzoyl moiety remained entirely solvent-exposed without productive protein contacts, explaining its inability to achieve effective target engagement.

These structural data, together with the biochemical inhibition data (IC_{50} = 2.96 nM for GPI; no inhibition by DFB), provide a comprehensive molecular explanation for the observed selectivity. The results will be presented as a new figure and table in the revised manuscript.

> *(7) Dietary carbohydrates could mask the metabolic effects of GP inhibition.*

Our new data showing no difference in feeding rate between ds*GP* and ds*GFP* groups addresses this concern from one angle: the metabolic changes we observe are not attributable to altered food intake. We will also add a discussion of the potential contribution

of dietary carbohydrates to glucose homeostasis and acknowledge this as a caveat in interpreting the metabolite data.

Minor points: All terminology errors ("gluconeogenolysis" → "gluconeogenesis"), typographical errors ("over over four decades"), and formatting inconsistencies will be corrected. We will clarify the metabolite normalization approach and improve figure labeling and pathway schematics.

> ***Reviewer #2 (Public review):***
>
> *(1) The central premise — that structural similarity among acylurea compounds implies shared molecular targets — is not supported by existing evidence.*

We agree that the original manuscript overstated the significance of the shared acylurea core as a predictor of common biological activity. In the revised manuscript, we will substantially restructure the Introduction to:

(1) Explicitly acknowledge the compelling genetic evidence from CRISPR/Cas9 experiments (Reference 5) establishing CHS as the primary site conferring BPU resistance.

(2) Reframe the study's objective: rather than proposing to "resolve" the BPU target controversy, the revised manuscript will focus on the systematic evaluation of GP as an independent insecticidal target and the discovery of a gluconeogenic compensation mechanism, questions that have scientific value independent of the BPU mechanism debate.

(3) Remove the claim that the study "resolves the primary hypothesis." The conclusion will instead state that our biochemical data demonstrate DFB does not inhibit PxGP, adding enzyme-level evidence to the existing genetic framework.

> *(2) Target selectivity among acylurea compounds is determined by side-chain composition, not the shared core.*

We fully agree, and our new structural data now provide a molecular explanation for this principle at the atomic level. Molecular docking reveals that both GPI and DFB anchor to PxGP through their common acylurea carbonyl groups (forming hydrogen bonds with Arg193), but diverge dramatically in their side-chain engagement: GPI's methoxyphenyl-methylurea moiety engages five additional residues across the dimer interface, while DFB's difluorobenzoyl group remains entirely solvent-exposed. The van der Waals energy difference ($\Delta\Delta G_{VDW}$ = −11.49 kcal/mol) quantitatively reflects this differential shape complementarity. These data directly support Reviewer 2's point and will be presented as new evidence in the revised manuscript.

> *(3) References 6–9 did not express CHS in cell-free assays.*

We will revise the relevant passage for greater precision. Our revised text will distinguish between (a) the absence of direct biochemical evidence for BPU-mediated CHS inhibition in cell-free systems and (b) the technical challenge of expressing and purifying functional CHS for such assays. This distinction will be stated more carefully to avoid any mischaracterization of the cited literature.

> *(4) The term "dataology" is non-standard.*

This term has been removed and replaced with "data." In accordance with eLife's policy on the use of AI tools and technology, we will include a statement in the Materials and Methods section declaring that AI-based language editing tools were used for English grammar and style refinement. All scientific content was generated entirely by the authors.

Summary of revisions

Concern	New data/revision	Status
GP enzyme activity after RNAi (R1 #4)	Coupled-enzyme assay at 24/48/72/96 h	**Complete**
Alternative glycogen catabolic enzymes (R1 #2)	RT-qPCR for *GBE* and *α-amylase*	**Complete**
Fitness cost assessment (R1 #3)	Feeding rate, larval weight, pupal weight	**Complete** (wing area in progress)
Structural evidence for GPI–PxGP interaction (R1 #8)	Homology model + Flare docking + MM/GBSA	**Complete**
Scope of BPU conclusion (R1 #5, R2)	Limited to DFB; CHS evidence acknowledged	In revision
RNAi recovery and non-essentiality (R1 #6)	Enzyme activity at recovery phase (96 h)	**Complete**
GPI concentration and pharmacokinetics (R1 #7)	Discussion added	In revision
Dietary compensation (R1 #9)	Feeding rate data + discussion	**Complete**
Narrative restructuring (R2)	Introduction and Discussion rewritten	In revision
Terminology and language (R1 minor, R2)	All corrections made; AI statement added	In revision

Author response table 1.

We are confident that the substantial new experimental data and restructured narrative will meaningfully strengthen the manuscript.

https://doi.org/10.7554/eLife.111144.1.sa0